Title

STUDY OF PHASE-MATCHED NORMAL AND UMKLAPP THIRD-HARMONIC GENERATION PROCESSES IN CHOLESTERIC LIQUID CRYSTALS

Authors

Shelton, J.W.
Shen, Y.R.

Publication Date

1971-08-01

Submitted to Physical Review

STUDY OF PHASE-MATCHED NORMAL AND UMKLAPP THIRD-HARMONIC GENERATION PROCESSES IN CHOLESTERIC LIQUID CRYSTALS

J. W. Shelton and Y.R. Shen

Aug. 1971

AEC Contract No. W-7405-eng-48

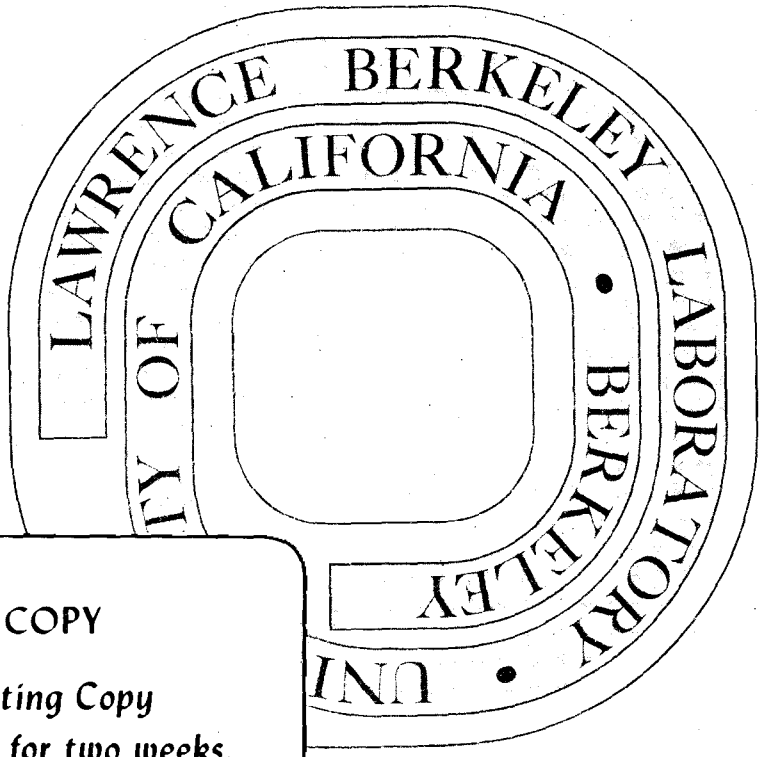

DISCLAIMER

Submitted to Physical Review

LBL-161
Preprint

UNIVERSITY OF CALIFORNIA

Lawrence Berkeley Laboratory
Berkeley, California

AEC Contract No. W-7405-eng-48

STUDY OF PHASE-MATCHED NORMAL AND UMKLAPP THIRD-HARMONIC GENERATION PROCESSES IN CHOLESTERIC LIQUID CRYSTALS

J. W. Shelton and Y. R. Shen

August 1971

Study of Phase-Matched Normal and Umklapp Third-Harmonic Generation Processes in Cholesteric Liquid Crystals

J. W. Shelton* and Y. R. Shen

Department of Physics, University of California and
Inorganic Materials Research Division, Lawrence Berkeley Laboratory,
Berkeley, California 94720

ABSTRACT

Using the model of Oseen and de Vries, we show that phase matching of optical third-harmonic generation can be achieved in a cholesteric liquid crystal with the help of the lattice momentum. Many different collinear phase matching conditions exist. In some cases, the phase-matched third-harmonic is generated in the same direction as the fundamental, and in some other cases, generated in the opposite direction. In many other cases, phase-matched third-harmonic generation requires the simultaneous presence of fundamental waves propagating in opposite directions. Analogous to electron-electron interaction in a periodic lattice, these processes can be identified as coherent, normal and umklapp third-harmonic generation processes. Experiments using a mode-locked Nd laser as the fundamental source verify the existence of most of the predicted phase-matching conditions. Our results agree very well with the theoretical predictions.

I. INTRODUCTION

Phase matching in nonlinear optical processes has long been a subject of interest. It not only has led to the successful development of useful nonlinear optical devices, but it has also helped in gaining information about linear and nonlinear optical properties of various materials. The usual technique of phase matching is to compensate the color dispersion by either linear birefringence,[1] or circular birefringence,[2] or anomalous dispersion of a dye.[3] However, we have recently demonstrated that phase matching can also be achieved in a periodic medium through compensation of the color dispersion by the lattice momentum.[4] The particular periodic medium we deal with is the cholesteric liquid crystalline material characterized by helical structure.[5]

In recent years, liquid crystals have become a field of interest for many research workers. While there is a large amount of work reported on their linear optical properties, reports on their nonlinear optical properties have been extremely rare. It was thought that since liquid crystals have large inherent birefringence, phase matching of harmonic generation would be possible in these materials and they could then be used as effective harmonic generators.[6] Experimental investigations of second-harmonic generation in nematic, smectic, and cholesteric liquid crystals have been made,[6-9] but there is no evidence of any discernible second-harmonic signal, suggesting that the molecular arrangement in these materials has an overall inversion symmetry.

Third-harmonic generation in liquid crystals is clearly not forbidden by symmetry. It has in fact been observed in a number of

liquid crystals by Goldberg and Schnur.[8,9] However, their attempt to achieve phase matching of third-harmonic generation in cholesteric liquid crystals has not been successful. Recently, using the model of Oseen[10] and de Vries[11] for cholesteric liquid crystals, we have been able to predict the helical pitch values at which collinear phase matching of third-harmonic generation would occur, and by tuning the pitch with temperature, have then been successful in observing the phase matching peaks as predicted.[4] In this paper, we would like to give a complete account of our work on the problem. We show that for third harmonic generation in a cholesteric liquid crystal, there could exist 15 different collinear phase matching conditions. We can divide them into three general classes. In the first class, both the fundamental and the phase-matched third-harmonic waves are propagating in the same direction as we normally expect. In the second class, the phase-matched third-harmonic is generated in a direction opposite to the fundamental. In the third class, the phase-matched third-harmonic is generated only when the fundamental waves are propagating simultaneously in both forward and backward directions. It is obvious from the requirement of momentum conservation that in the last two cases, phase matching can only be achieved if the momentum mismatch between the fundamental and the third-harmonic can be absorbed by the medium. In fact, in most cases here, phase matching is achieved through compensation of color dispersion by the lattice momentum of the periodic medium as we shall see later.

In Section II, we give a brief review of the linear optical properties of a cholesteric liquid crystal. We point out that propagation

of light waves along the helical axis in such a medium is analogous to propagation of electron waves in a one-dimensional periodic lattice. What we have here is Bloch photons instead of Bloch electrons. In Section III, we describe the theory of third-harmonic generation in a cholesteric liquid crystal. We show that collinear phase matching is possible with the help of the lattice momentum for many different mode combinations. Clearly, such phase-matched third-harmonic generation processes fall into the category of nonlinear Bragg diffraction.[12] In analogy to umklapp processes of electrons in solids,[13] they can also be called coherent, optical, umklapp processes. In Section IV, we describe the experimental arrangement and show that the results agree with theoretical predictions. Finally, in Section V, we discuss the effects of many experimental difficulties on the observed phase-matched third-harmonic generation.

II. THEORY OF LINEAR OPTICAL WAVE PROPAGATION IN A CHOLESTERIC LIQUID CRYSTAL

Liquid crystals are generally composed of long, anisotropic organic molecules.[5] The so-called nematic structure has long-range order in molecular orientation with the long molecular axes aligned more or less parallel to one another, although the molecules are fairly free to translate and to rotate about their long axes. The cholesteric structure is simply a twisted version of the nematic. It is formed by twisting the nematic structure about an axis normal to the molecular alignment so as to have an overall helical structure. The helical pitch is a function of composition, temperature, fields, and

other external perturbations, and usually varies from ± 0.2 μm to essentially infinity. Because of their helical structure, cholesteric liquid crystals have some interesting optical properties. In particular, the optical Bragg reflection gives rise to their grating characteristics. We shall see in the next section that these materials also have interesting nonlinear optical properties arising from nonlinear optical Bragg reflection.

The theory of linear wave propagation in a cholesteric liquid crystal has been well developed by Oseen[10] and de Vries.[11] They assume that a cholesteric liquid crystal can be treated as a twisted birefringent medium characterized by a dielectric tensor $\underset{\approx}{\varepsilon}(z)$ periodic in z.

$$\underset{\approx}{\varepsilon}(z) = \begin{pmatrix} \bar{\varepsilon}(1+\alpha\cos(4\pi z/p)) & \bar{\varepsilon}\alpha\sin(4\pi z/p) & 0 \\ \bar{\varepsilon}\alpha\sin(4\pi z/p), & \bar{\varepsilon}(1-\alpha\cos(4\pi z/p)) & 0 \\ 0, & 0, & \varepsilon_\eta \end{pmatrix} \qquad (1)$$

where $\bar{\varepsilon} = (\varepsilon_\xi+\varepsilon_\eta)/2$, $\alpha = (\varepsilon_\xi-\varepsilon_\eta)/2\bar{\varepsilon}$,

ε_ξ and ε_η are the principal dielectric constants in the directions parallel and perpendicular to the molecular alignment respectively, and p is the helical pitch. Note that in this model, the dielectric tensor $\underset{\approx}{\varepsilon}(z)$ has a period of p/2 rather than p.

Although the general solution for light propagation in any direction is available,[14] we shall consider here only propagation along the helical (z-) axis. The corresponding wave equation for monochromatic light is given by

$$[(\partial^2/\partial z^2) + (\omega^2/c^2)\,\underset{\approx}{\varepsilon}(z)] \cdot \underset{\sim}{E}(z) = 0. \qquad (2)$$

This equation with a position-dependent dielectric constant is most easily solved by first applying to the equation a rotational transformation

$$R\ (\theta = 2\pi z/p) = \begin{pmatrix} \cos\theta, & \sin\theta, & 0 \\ -\sin\theta, & \cos\theta, & 0 \\ 0, & 0, & 1 \end{pmatrix}. \tag{3}$$

Physically, the rotational transformation is to untwist the twisted helical structure, so that in the rotating frame the medium now appears to be a simple birefringent material with a dielectric tensor $\underset{\approx}{\varepsilon}_T = \underset{\approx}{R} : \underset{\approx}{\varepsilon}(z) : \underset{\approx}{R}^{-1}$ independent of z. This technique is analogous to the rotational transformation technique used in magnetic resonance.[15] After the transformation, Eq. (2) becomes:

$$\left[\frac{\partial^2}{\partial z^2} + \frac{4\pi}{p} \underset{\approx}{g} \frac{\partial}{\partial z} - \left(\frac{2\pi}{p}\right)^2 + \frac{\omega^2}{c^2} \underset{\approx}{\varepsilon}_T \right] \cdot \underset{\sim}{E}_T = 0 \tag{4}$$

where

$$\underset{\approx}{g} = \begin{pmatrix} 0 & -1 & 0 \\ 1 & 0 & 0 \\ 0 & 0 & 0 \end{pmatrix}, \qquad \varepsilon_T = \begin{pmatrix} \varepsilon_\xi & 0 & 0 \\ 0 & \varepsilon_\eta & 0 \\ 0 & 0 & \varepsilon_\eta \end{pmatrix}.$$

The above equation can now be solved readily. Let

$$\underset{\sim}{E}_T = \sum_{j=\pm} (\mathscr{E}_\xi \hat{\xi} + \mathscr{E}_\eta \hat{\eta})_j \exp(ik_j z - i\omega t) \tag{5}$$

where $\hat{\xi} = \hat{x} \cos(2\pi z/p) + \hat{y} \sin(2\pi z/p)$ and $\hat{\eta} = -\hat{x} \sin(2\pi z/p) + \hat{y} \cos(2\pi z/p)$ are unit vectors parallel and perpendicular to the molecular alignment in the plane at z respectively. We then find

$$k_{\pm}^{(\omega)} = (\omega\bar{\varepsilon}^{1/2}/c)m_{\pm}$$

$$(m_{\pm})^2 = (\lambda'^2+1) \pm (4\lambda'^2+\alpha^2)^{1/2}, \quad \lambda' = 2\pi c/\omega p\bar{\varepsilon}^{1/2},$$

$$(\mathscr{E}_\eta/\mathscr{E}_\xi)_{\pm} \equiv if_{\pm} = i2m_{\pm}\lambda'/[m_{\pm}^2 + \lambda'^2 + (\alpha - 1)]. \tag{6}$$

The magnitudes of $\mathscr{E}_{\xi+}$ and $\mathscr{E}_{\xi-}$ are determined by the boundary conditions. The Poynting vectors for the two modes are

$$\underset{\sim}{S}_{\pm} = (|\mathscr{E}_{\pm}|^2 c\bar{\varepsilon}^{1/2}/2\pi) \frac{\mathrm{Re}[q+|f|^2/q]_{\pm}}{1+|f_{\pm}|^2} \hat{z} \tag{7}$$

where $$q_{\pm} = (m_{\pm}/\bar{\varepsilon}^{1/2}) - \lambda' f_{\pm}$$

and $$|\varepsilon_{\pm}|^2 \equiv (|\mathscr{E}_\xi|^2 + |\mathscr{E}_\eta|^2)_{\pm}.$$

It can be shown that for the "-" mode in the region of $\lambda'^2 > (1+|\alpha|)$, a forward propagating wave (with $\underset{\sim}{S}_-$ in the $+\hat{z}$ direction) actually corresponds to $m_- < 0$ (indicating a negative phase velocity in the rotating frame). We also remark that here the two modes are generally not orthogonal since $\underset{\sim}{E}_{T+} \cdot \underset{\sim}{E}_{T-} \neq 0$. This non-orthogonal property does not affect the linear wave propagation, but affects the nonlinear wave propagation slightly as we shall see in the next section.

The above solutions describe the characteristics of linear wave propagation in a cholesteric liquid crystal along the helical axis. In particular, if $|\lambda'^2 - 1| < |\alpha|$, then m_- is purely imaginary, and the corresponding wave should be totally reflected. We realize that $\lambda' \approx 1$ or $\lambda = 2\pi c/\omega\bar{\varepsilon}^{1/2} = p$ ($|\alpha| \ll 1$ usually) is just the condition for Bragg reflection from the helical structure. If we transform Eq. (5) back into the lab frame, we have

$$\underset{\sim}{E}_{\pm} = \underset{\approx}{R}^{-1}\, \underset{\sim}{E}_{T\pm}$$

$$= \left[\frac{\hat{x}+i\hat{y}}{\sqrt{2}} A_{R\pm} + \frac{\hat{x}-i\hat{y}}{\sqrt{2}} A_{L\pm}\, e^{i4\pi z/p}\right] \&_{\xi\pm} \exp[i(m_{\pm}\omega\bar{\varepsilon}^{1/2}/c - 2\pi/p)z - i\omega t] \tag{8}$$

where $A_{L\pm} = (1+f_{\pm})/\sqrt{2}$

$A_{R\pm} = (1-f_{\pm})/\sqrt{2}$.

This equation shows that in the lab frame, each mode is a superposition of two components, a left circularly polarized one with an effective refractive index $n_{L\pm} = (m_{\pm} - \lambda')\bar{\varepsilon}^{1/2}$ and a right circularly polarized one with $n_{R\pm} = (m_{\pm} + \lambda')\bar{\varepsilon}^{1/2}$. The ratios of A_R to A_L for the two modes are plotted in Fig. 1. We notice that the "+" mode is always nearly circularly polarized as long as $\lambda'^2 \gg \alpha^2$, and the "-" mode is nearly circularly polarized everywhere except for $\lambda'^2 < \alpha^2$ and for $(1 - |\alpha|) < \lambda'^2 < (1+|\alpha|)$. For a right-handed cholesteric liquid crystal, the dominant components for the two modes are A_{L+} and A_{R-} respectively. Since these two dominant circular components have different phase velocities ($n_{L+} \neq n_{R-}$), the medium possess an optical activity

$$R(\text{radians/unit length}) = (\omega/2c)\,(n_{R-} - n_{L+})$$

$$\simeq -\pi\alpha^2/4p\lambda'^2\,(1-\lambda'^2). \tag{9}$$

It is well known that the optical activity of a cholesteric liquid crystal can be as high as 300 rad/cm.[5] The above equation is of course not valid for $\lambda' \sim 0$ and 1, since then our approximation breaks down.

We can also understand the problem by recognizing the analog between this problem and the problem of electron wave propagation in a one-dimensional periodic lattice. The latter problem is well presented in elementary textbooks on solid-state physics.[13] We can use the same approach to solve our problem directly in the lab frame.

According to Bloch's theorem,[13] the wave solution can be written in the form

$$\underset{\sim}{E} = \underset{\sim}{u}(\kappa,z)\, \exp[i\kappa z - i\omega t] \tag{10}$$

where $\underset{\sim}{u}(\kappa,z)$ is a periodic function of z with a period of p/2, and κ is limited to the first Brillouin zone between $2\pi/p$ and $-2\pi/p$. Substitution of Eq. (10) into Eq. (2) yields

$$[\frac{\partial^2}{\partial z^2} + 2i\kappa\frac{\partial}{\partial z} - \kappa^2 + \frac{\omega^2}{c^2}\underset{\approx}{\varepsilon}(z)] \cdot \underset{\sim}{u}(\kappa,z) = 0. \tag{11}$$

We can expand both $\underset{\sim}{u}(\kappa,z)$ and $\underset{\approx}{\varepsilon}(z)$ into Fourier series

$$\begin{aligned} \underset{\sim}{u}(\kappa,z) &= \sum_G \underset{\sim}{C}_G(\kappa)\, \exp(iGz) \\ \underset{\approx}{\varepsilon}(z) &= \sum_G \underset{\approx}{\varepsilon}_G\, \exp(iGz) \end{aligned} \tag{12}$$

where $G = N(4\pi/p)$, with N being any integer, is a reciprocal lattice vector. Eq. (11) then becomes

$$(\kappa+G)^2 \underset{\sim}{C}_G - (\omega^2/c^2) \sum_{G'} \underset{\approx}{\varepsilon}_{G'} \cdot \underset{\sim}{C}_{G-G'} = 0. \tag{13}$$

This set of equations with different G's is most easily solved by expressing the vectors and tensors in the circular coordinates $(\hat{x} + i\hat{y})/\sqrt{2}$, $(\hat{x} - i\hat{y})/\sqrt{2}$, and $\hat{z}$. There, we have

$$\underset{\approx}{\varepsilon}(z) = \bar{\varepsilon}\begin{pmatrix} 1, & \alpha\exp(-i4\pi z/p), & 0 \\ \alpha\exp(i4\pi z/p), & 1, & 0 \\ 0, & 0, & 1 \end{pmatrix} \tag{14}$$

which has only three Fourier components $\underset{\approx}{\varepsilon}_G$ with G = 0, and $\pm 4\pi/p$. It is then simple to solve Eq. (13). We obtain

$$(\kappa_\pm + G + 2\pi/p)^2 = (\omega^2\bar{\varepsilon}/c^2)[1+\lambda' z \pm (4\lambda'^2+\alpha^2)^{1/2}]$$

$$\underset{\sim}{E} = [(1+f_\pm)(\hat{x}+i\hat{y}) + (1-f_\pm)(\hat{x}-i\hat{y})\exp(i4\pi z/p)](\mathcal{E}_{\xi\pm}/2) \times$$

$$\times \exp[i(\kappa_\pm + G)z - i\omega t]. \tag{15}$$

These solutions are identical to those we obtained before in Eqs. (6) and (8), with $\kappa_\pm + G + 2\pi/p = m_\pm \omega \bar{\varepsilon}^{1/2}/c$, remembering that $|\kappa_\pm| \leq 2\pi/p$.

We can find the dispersion curves for the two modes from Eq. (15). Either extended or reduced zone scheme can be used. Analogous to the band gap in the electronic band structure, the dispersion curve for the negative mode has a gap between $\lambda'^2 = (1-|\alpha|)$ and $(1+|\alpha|)$ at $\kappa = \pm 2\pi/p$. This is just the reflection band of the cholesteric liquid crystal. However, in contrast to the case of electrons in a periodic

lattice,[13] we have here only one gap for only one of the two normal modes.

Usually, one prepares a sample of cholesteric liquid crystal by holding the material between two glass substrates. In order to know how each mode is being excited, we have to solve the problem with the proper boundary conditions. This has been done by de Vries.[11] Using his result, we plot in Fig. 2, as a function of λ', the polarizations of the incident fields which should feed exclusively into each of the two modes. For $\lambda'^2 >> |\alpha|$, both of them are close to circular polarization. The polarization of the incident field which feeds into the "-" mode should have the same handedness as the helicity of the cholesteric structure.

Knowing the characteristics of linear wave propagation, we can then discuss the nonlinear optical effects in a cholesteric liquid crystal. In the following section, we shall consider the problem of third-harmonic generation along the helical axis in such a medium. Emphasis is on the derivation of collinear phase-matching conditions.

III. THEORY OF THIRD-HARMONIC GENERATION IN CHOLESTERIC LIQUID CRYSTALS

A. Third-Harmonic Generation

Third-harmonic generation along the helical axis in a cholesteric medium is governed by the nonlinear wave equation

$$[\frac{\partial^2}{\partial z^2} + (\frac{3\omega}{c})^2 \underset{\approx}{\varepsilon}(z,3\omega)] \cdot \underset{\sim}{E}(z,3\omega) = -4\pi(\frac{3\omega}{c})^2 \underset{\sim}{P}^{(3)}(z,3\omega) \tag{16}$$

where the nonlinear polarization $\underset{\sim}{P}^{(3)}(z,3\omega)$ has the form

$$\underset{\sim}{P}^{(3)}(z,3\omega) = \underset{\approx}{\chi}^{(3)}(z,3\omega) : \underset{\sim}{E}(z,\omega)\ \underset{\sim}{E}(z,\omega)\ \underset{\sim}{E}(z,\omega). \tag{17}$$

The nonlinear susceptibility tensor $\underset{\approx}{\chi}^{(3)}(z,3\omega)$ is also a periodic function of z.

In the rotating frame, Eq. (16) becomes

$$[\frac{\partial^2}{\partial z^2} + \frac{4\pi}{p}\underset{\approx}{\sigma}\frac{\partial}{\partial z} - (\frac{2\pi}{p})^2 + (\frac{3\omega}{c})^2 \underset{\approx T}{\varepsilon}] \cdot \underset{\sim T}{E}(z,3\omega) = -4\pi(\frac{3\omega}{c})^2 \underset{\sim T}{P}^{(3)} \tag{18}$$

with

$$\underset{\sim T}{P}^{(3)} = -4\pi(\frac{3\omega}{c})^2 \underset{\approx T}{\chi}^{(3)} \cdot \underset{\sim T}{E}(z,\omega)\ \underset{\sim T}{E}(z,\omega)\ \underset{\sim T}{E}(z,\omega).$$

The transformed $\underset{\approx T}{\chi}^{(3)}$ is now independent of z and has the form for a birefringent material with four independent elements.[17] Then, the components of $\underset{\sim T}{P}^{(3)}$ along $\hat{\xi}$ and $\hat{\eta}$ are

$$P_{T\xi}^{(3)}(3\omega) = C_{11}\, E_\xi(\omega)\, E_\xi(\omega)\, E_\xi(\omega) + C_{12}\, E_\xi(\omega)\, E_\eta(\omega)\, E_\eta(\omega)$$

$$P_{T\eta}^{(3)}(3\omega) = C_{21}\, E_\eta(\omega)\, E_\xi(\omega)\, E_\xi(\omega) + C_{22}\, E_\eta(\omega)\, E_\eta(\omega)\, E_\eta(\omega). \qquad (19)$$

To solve Eq. (18), we use the usual slowly-varying-amplitude approximation.[16] Let

$$\underset{\sim}{E}_T(z,3\omega) = [\hat{e}_+ \mathcal{E}_+(z, 3\omega) \exp(ik_+ z) + \hat{e}_- \mathcal{E}_- (z,3\omega) \exp(ik_- z)]$$

$$\times \exp(-i\omega t) \qquad (20)$$

where

$$|\partial^2 \mathcal{E}_+/\partial z^2| \ll |2k_+ \partial \mathcal{E}_+/\partial z|, \quad |\partial^2 \mathcal{E}_-/\partial z^2| \ll |2k_- \partial \mathcal{E}_-/\partial z|.$$

The expressions for the unit vectors $\hat{e}_+$ and $\hat{e}_-$, obtained from Eqs. (5) and (6), are

$$\hat{e}_\pm = [1/(1+|f_\pm|^2)^{1/2}]\ (\hat{\xi} + i f_\pm \hat{\eta}). \qquad (21)$$

Then, substitution of Eq. (20) into Eq. (18) yields

$$\sum_j [2ik_j + \frac{4\pi}{p} \underset{\approx}{\sigma}]\ \hat{e}_j \exp(ik_j z - i3\omega t)\ \frac{\partial}{\partial z} \mathcal{E}_j(z,3\omega) = -4\pi(\frac{3\omega}{c})^2 \underset{\sim}{P}_T^{(3)}. \qquad (22)$$

The scalar products of $\hat{e}_1^\dagger$ and $\hat{e}_2^\dagger$ with the above equation give

$$A \exp(ik_+ z) \frac{\partial}{\partial z} \mathcal{E}_+ + B \exp(ik_- z) \frac{\partial}{\partial z} \mathcal{E}_- = -4\pi\left(\frac{3\omega}{c}\right)^2 \hat{e}_+^\dagger \cdot \underset{\sim}{P}_T^{(3)}$$

$$C \exp(ik_+ z) \frac{\partial}{\partial z} \mathcal{E}_+ + D \exp(ik_- z) \frac{\partial}{\partial z} \mathcal{E}_- = -4\pi\left(\frac{3\omega}{c}\right)^2 \hat{e}_-^\dagger \cdot \underset{\sim}{P}_T^{(3)} \qquad (23)$$

where

$$A = 2ik_+ + (4\pi/p)\hat{e}_+^\dagger \cdot \underset{\approx}{\sigma} \cdot \hat{e}_+$$

$$B = \hat{e}_+^\dagger \cdot [2ik_- + (4\pi/p)\underset{\approx}{\sigma}] \cdot \hat{e}_-$$

$$C = \hat{e}_-^\dagger \cdot [2ik_+ + (4\pi/p)\underset{\approx}{\sigma}] \cdot \hat{e}_+$$

$$D = 2ik_- + (4\pi/p)\hat{e}_-^\dagger \cdot \underset{\approx}{\sigma} \cdot \hat{e}_-.$$

From Eq. (23), we can easily obtain expressions for $\partial\mathcal{E}_+/\partial z$ and $\partial\mathcal{E}_-/\partial z$. Then, in the low depletion limit using the parametric approximations,[16] we find

$$\mathcal{E}_+(z=\ell,3\omega) = 4\pi\left(\frac{3\omega}{c}\right)^2 \left(\frac{D\hat{e}_+^\dagger - B\hat{e}_-^\dagger}{AD - BC}\right) \cdot \underset{\approx}{\chi}_T^{(3)} : \sum_{\ell,m,n=\pm} \hat{e}_\ell \hat{e}_m \hat{e}_n \mathcal{E}_\ell(\omega)\mathcal{E}_m(\omega)\mathcal{E}_n(\omega)$$

$$\frac{\sin(\Delta k_{+\ell mn}\ell/2)}{\Delta k_{+\ell mn}/2} \exp(i\Delta k_{+\ell mn}\ell/2)$$

$$\mathcal{E}_-(z=\ell,3\omega) = 4\pi\left(\frac{3\omega}{c}\right) \left(\frac{A\hat{e}_-^\dagger - C\hat{e}_+^\dagger}{AD - BC}\right) \cdot \underset{\approx}{\chi}_T^{(3)} : \sum_{\ell,m,n=\pm} \hat{e}_\ell \hat{e}_m \hat{e}_n \mathcal{E}_\ell(\omega)\mathcal{E}_m(\omega)\mathcal{E}_n(\omega)$$

$$\frac{\sin(\Delta k_{-\ell mn}\ell/2)}{\Delta k_{-\ell mn}/2} \exp(i\Delta k_{-\ell mn}\ell/2) \qquad (24)$$

where $\Delta k_{\pm\ell mn} = k_\ell^{(\omega)} + k_m^{(\omega)} + k_n^{(\omega)} - k_\pm^{(3\omega)}$.

Note that the waves can propagate along the helical axis in either direction, and, correspondingly, the wave vectors k can be positive or negative. The generated third-harmonic intensity is given by Eq. (7), which is of course independent of the coordinate system we choose. If the beam has a finite cross-section, then the total third-harmonic power is[18]

$$P_{\pm}(3\omega) = \int S_{\pm}(3\omega, x,y)dxdy. \tag{25}$$

B. Phase Matching or Conservation of Linear Momentum

Third-harmonic generation is most efficient when a certain phase-matching condition $\Delta k_{\pm \ell mn} = 0$ is satisfied. When this happens, the corresponding phase-matched term dominates over the other terms in the summation in Eq. (24). Since we allow both the fundamental and the third harmonics to be in either mode and to propagate along the z-axis in either direction, we can have many different phase matching conditions in a cholesteric liquid crystal by taking all possible sign combinations in the following equation:

$$\pm|k_{\pm}^{(3\omega)}| = \pm|k_{\pm}^{(\omega)}| \pm |k_{\pm}^{(\omega)}| \pm |k_{\pm}^{(\omega)}|. \tag{26}$$

Through the dependence of k on the pitch p, the phase matching conditions can be achieved by adjusting p. However, Eq. (26) cannot be satisfied for all the 40 different sign combinations. If we assume $\bar{\varepsilon}^{(3\omega)} > \bar{\varepsilon}^{(\omega)}$, then only 12 of them are possible, and another 3 can be conditionally satisfied. They are listed in Table I, where a super bar

on k indicates a backward propagating mode ($\bar{k} = -k$).

Physically, phase matching is achieved here through compensation of momentum mismatch by the lattice momentum. This can be seen as follows. We realize from Eq. (6) that for the "+" mode in the region $\lambda'^2 >> \alpha^2$ and for the "-" mode in the region $\alpha^2 << \lambda'^2$ and $(1-\lambda')^2 >> \alpha^2/4\lambda'$, the wave vectors $|k_\pm|$ can be well approximated by

$$|k_\pm| = |k_o \pm 2\pi/p| \tag{27}$$

where $k_o^{(\omega)} = \omega\bar{\varepsilon}^{1/2}/c$ is the average wave vector. This approximation is excellent for the first 11 mode combinations in Table I, and is marginal for the 12th, since α is usually about 0.03. Consequently, using Eq. (27), we can rewrite these phase matching conditions in terms of $k_o^{(\omega)}$, $k_o^{(3\omega)}$, and the unit lattice momentum $Q = 4\pi/p$ as shown in the second column of Table I. We notice that in all cases the average momentum mismatch between the fundamental and the third harmonic is compensated by the lattice momentum Q or 2Q. From these expressions we can easily calculate the values of p satisfying the phase matching conditions if $\bar{\varepsilon}^{(3\omega)}$ and $\bar{\varepsilon}^{(\omega)}$ for the material are known. For the materials we have used in our experimental investigation, $\bar{\varepsilon}^{(3\omega)}$ and $\bar{\varepsilon}^{(\omega)}$ are typically 2.30 and 2.18 respectively and $\alpha \approx 0.03$. The corresponding pitches for phase matching of different mode combinations are given in the last column of Table I for illustration.

The approximation of Eq. (27) is not valid for the last three mode combinations in Table I. It is clear that since the momentum mismatches in these cases are small, the pitches for phase matching

must be long. Then, as seen from Eq. (6), the birefringence factor α can no longer be neglected in the expression for $k_{\pm}$. In fact, the phase matching conditions for these last three mode combinations may not always be satisfied. The conditions for phase matching in these cases are given in Table I.

The more rigorous interpretation of phase matching or momentum matching here is to use the concept of waves propagating in a periodic medium. As we showed in the last section, the em waves propagating in such a medium should have the form of Bloch functions, Eq. (10), with κ being the wave vectors. It is really κ's which we should use in discussing conservation of linear momentum or phase matching. In the third column of Table I, we write the phase matching conditions for the various mode combinations in terms of κ's. Again, we notice that in many cases, the mismatches between κ's are compensated by the lattice momentum $Q = 4\pi/p$. In analogy to electron-electron interaction in a periodic lattice, these phase-matched processes can then be called the coherent optical umklapp processes. They are coherent since third harmonic generation is a coherent process. For the other cases where phase matching can be achieved with no lattice momentum involved, the processes are correspondingly the normal processes.[13] It is clear that we can also express the phase matching conditions for the last three mode combinations in terms of κ's and $G = N(4\pi/p)$, but the integer N in these cases depend on the actual values of $\bar{\epsilon}$ and α.

Finally, we realize that as $p \to \infty$, the cholesteric medium becomes a simple birefringent medium, and the waves propagating along the z axis have two linearly polarized modes. The last three

combinations in Table I can then be written as

$$3\,[\varepsilon_\eta^{1/2}(3\omega) - \varepsilon_\eta^{1/2}(\omega)\,] = n[\varepsilon_\xi^{1/2}(\omega) - \varepsilon_\eta^{1/2}(\omega)] \qquad (28)$$

with n = 3, 2, 1 respectively. Eq. (28) shows that the color dispersion is balanced by birefringence. This is how phase matching is usually achieved in a birefringent medium.

It has been suggested that phase matching can probably be achieved in cholesteric liquid crystals through compensation of color dispersion by circular birefringence because of their large optical rotary power.[2] This would be the case if, in the mode combinations #12 - #15 of Table I with all waves propagating in the same direction, the modes were circularly polarized. However, in all these cases, because of the large pitches for possible phase matching, the modes are far from being circularly polarized.

C. Conservation of Angular Momentum

The optical fields can also exchange angular momentum with the cholesteric medium in the third-harmonic generation process. The medium has a local two-fold symmetry about the helical axis, and therefore in the process of converting three fundamental photons into one third-harmonic photon can exchange an angular momentum in units of $2\hbar$ with the optical fields.[19] Since each photon of circular polarization carries an angular momentum of $\pm\hbar$, any polarization combination in the third-harmonic generation satisfies the requirement of conservation of angular momentum. Thus, for example, for the 6th mode combination in Table I, the modes involved are nearly circularly polarized, and

creation of a third-harmonic photon leaves an angular momentum of $2(2\hbar)$ to the medium. Similarly, one can show that conservation of angular momentum is satisfied for all other mode combinations.

In the next section, we show our experimental results, which verify the above theoretical predictions.

IV. EXPERIMENTS

A. Sample Preparation and Related Measurements

In our experiments we have used a number of different cholesteric liquid-crystalline materials in order to observe the various predicted phase-matching peaks in third-harmonic generation at a convenient temperature. Most of the phase matching conditions (#1 - #11) in Table I require a cholesteric liquid crystal with a pitch less than 1.5 μm. To observe them, we used mixtures of cholesteryl oleyl carbonate, cholesteryl nonanoate, and cholesteryl chloride.[20] The ratio of cholesteryl oleyl carbonate to cholesteryl nonanoate was unity by weight in all our mixtures, but the concentration of cholesteryl chloride varied for different phase-matching conditions as listed in Table II. Figure 3 shows from our measurements the pitch as a function of the concentration of cholesteryl chloride at 20°C and 40°C. The temperature variation of the pitch between 20°C and 40°C can be crudely estimated from the two curves in Fig. 3.[21] The sample used to observe the 12th phase matching condition was a mixture of cholesteryl chloride and cholesteryl myristate (1.75 = 1 by weight).[20] This mixture has a pitch which is

variable from -1.7 μm to ± ∞ to +2μm by varying the temperature from 20°C to 68°C. (A negative pitch denotes a left-handed helical structure. This allowed us to observe the phase-matching peaks at both -17.3 μm and +17.4 μm.

Samples were prepared by placing a few drops of the mixture on a clean, rubbed glass window. A second window was then pressed upon the first with a ring of teflon or mylar as the spacer. Clear and uniform samples up to ~ 250 μm in thickness were obtained with the helical axis more or less perpendicular to the normal of the surface. Under a polarizing microscope, however, small regions of > 10 μm in size were discernable with slightly different optical properties, indicating domains with somewhat different orientations of the helical axis. Bragg reflection of a collimated beam from such a sample spread over a cone of about 12°, suggesting that the helical axis had a distribution of around 6° about the normal of the surface. Each domain, however, seemed to extend over the entire thickness of the sample. The effect of multi-domains on phase-matched third-harmonic generation will be discussed in Section V. Most of our experiments were done with 130 μm thick samples. Samples with randomly oriented domains were easily obtained by increasing the sample thickness or by subjecting samples to thermal shocks.

Prediction of the precise pitches for phase matching requires the measurement of $\bar{\varepsilon}$ and α(see Eqs. (26) and (6)). Since $\bar{\varepsilon}$ is an average over the two principal dielectric constants in the ordered phase, we measured $\bar{\varepsilon}(\omega)$ and $\bar{\varepsilon}(3\omega)$ with λ_ω = 1.06μm in the isotropic liquid phase where the random orientations of the molecules gives the

desired average. It was assumed that the small variation of $\bar{\varepsilon}$ due to temperature and phase difference between the liquid and the liquid crystal phases could be neglected. We used the prism method with a mercury-arc lamp as the light source and a filtered photomultiplier tube as the detector.[22] The results are given in Table II.

The birefringence factor α is most easily obtained by measuring the optical activity of the sample (see Eq. (9)). We measured the optical activity at the He-Ne laser frequency (6328 Å) and assumed a negligible dispersion for α. For all samples, α decreased with increasing temperature.[4,23] An example is shown in Fig. 4. In Table II, we list our measured values of α for the various mixtures at the temperatures where phase matching occurs. We realize, from our discussion in the last section, that all these phase matching conditions in Table II do not depend critically on the values of α. Therefore, the measurements of α here need not be very accurate.

From the measured values of $\bar{\varepsilon}$ and α, we can calculate the pitches for phase matching for the various mode combinations using Eqs. (6) and (26). These predicted pitches are also given in Table II.

We used three different techniques to measure the pitches of our samples. For pitches significantly larger than optical wavelengths, two techniques are convenient. Direct observation of the samples under a polarizing microscope can reveal the periodic structure as alternating light and dark bands,[24] whose periodicity is $p/2$. This method requires knowing the orientation of the helical axis in the region being examined, and the axis must have a component perpendicular to the microscope axis. A generally more convenient technique is the diffraction method.[25]

In a sample with uniformly oriented helical axes, a laser beam propagating normal and polarized normal to the helical axis will generate diffraction spots at angles θ with respect to the helical axis satisfying $\cos\theta = 2N\lambda_o/p$, where N is an integer and $\lambda_o = 2\pi\omega/c$. If the sample has many domains of different orientations, then diffraction arcs or rings will appear. From the diffraction pattern, one can find the pitch. For pitches in the vicinity of the visible spectrum, the pitch may be deduced from measurements of reflectivity or transmissivity as a function of wavelength. The position of the center of the reflection band corresponds to $p = 2\pi c/\omega\bar{\varepsilon}^{1/2}$. This is most easily measured in thin ($\lesssim$ 10 μm) samples, for which the band has a true peak; in thicker samples, there is a broad band of total reflectivity for the "-" mode, making the center of the band more difficult to determine.

In the regions where the above three techniques of pitch measurements overlap, we found good agreement. Temperature dependences of the pitch for the various mixtures were also measured. An example is given in Fig. 5 for the mixture used to observe the 12th phase matching condition. In Table III, we list the temperatures at which the predicted phase-matching would occur in the various mixtures. Most of the uncertainty in the predicted temperatures arose from the measurements of $\bar{\varepsilon}$, which entered the theoretical expressions explicitly and also implicitly through the experimentally determined α and p. Table III also gives the rate of change of pitch with temperature in the phase-matching regions.

B. Experimental Arrangements for Third-Harmonic Generation

We used a mode-locked Nd:glass laser as the fundamental pump source. A typical pulse train lasted about 200 ns with the individual pulses separated by about 7 ns. The total energy in each train was about 0.03 joule and the pulse width of individual pulses was about 7 ps as measured by two-photon fluorescence technique.[26] The beam diameter was about 2 mm. Mode-locked pulses were used in the experiments because their high peak intensities greatly enhanced the total third-harmonic power generated.

The experimental arrangement for measuring phase-matched third-harmonic generation with the fundamental propagating only in one direction is shown in Fig. 6. The third-harmonic generated either forward or backward was detected by a photomultiplier after the appropriate filters. The setup with the fundamental propagating in both directions is shown in Fig. 7. A movable mirror was used to obtain laser light propagating in the backward direction. A stressed fused silica plate was used as a variable retardation plate in front of the mirror to control the polarization of the backward propagating laser beam. The laser beam was always circularly polarized for two reasons. First, as we discussed in Section II, circular polarizations are nearly the optimum polarizations for the incoming beam to excite the normal modes in all the samples of interest to us, and second, since no third-harmonic can be generated in an isotropic medium by a circularly polarized beam,[27] this eliminates the background third harmonic radiation generated from various components except the liquid crystal along the optical path. The third-harmonic blocking

filters in front of the quarter-wave plate are necessary to eliminate the third harmonic generated before the quarter-wave plate. The samples were immersed in a water bath with temperature controlled to within ± 0.02°C. Typically the temperature was swept very slowly (0.1 to 0.01 °C/min) through the predicted phase-matching region. In order to minimize fluctuations,[28] the third-harmonic signal from the liquid crystalline sample was always normalized against the reference third-harmonic signal generated in a phase-matched solution of fuchsin basic dye dissolved in hexafluoracetone sesquihydrate.[3]

C. Experimental Results on Phase-Matched Third-Harmonic Generation.

Consider first the phase-matching condition $3k_+^{(\omega)} = k_+^{(3\omega)}$ (#12 in Table II). The setup in Fig. 6 was used for the experiments. Since the pitch of the sample can vary from left to right handedness, there should be two phase-matching peaks. The one at -17.3 μm (49.4°C) should be generated by right circularly polarized fundamental waves and the other at +17.4 μm (54.2°C) should be generated by left circularly polarized fundamental waves. The generated third harmonics should have opposite polarizations in the two cases. The experimental results are shown in Fig. 8. The two peaks appear at temperatures within 0.1°C of the predicted phase-matching temperatures. They were generated respectively by right and left circularly polarized laser light as predicted. The theoretical phase-matching curve calculated by assuming monochromatic pump waves in a uniformly ordered liquid crystal is shown in Fig. 8. The experimental peaks are definitely broader with no clear fine structure at the wings. The difference between theory and experiment will be discussed in the next section. Since the molecular structures for $p < 0$ and $p > 0$ are different and $\underset{\approx}{\chi}^{NL}$ could vary accordingly, we would not

expect the two phase-matching peaks to have the same magnitude. Experimentally, we found that the two peaks were different in height, but their difference was within the 20% experimental accuracy. We also found that the two peaks were actually oppositely polarized. They had an elliptical polarization with the ratio of the two circularly polarized components being 5 ± 1. The theoretical ratio, derived from Eq. (8) or (15) is 4.8. Comparison of the phase-matched third-harmonic signals from the liquid crystal and from the fuchsin basic dye solution yields $I_{LQ}^{(3\omega)}/I_{Dye}^{(3\omega)} \sim 0.1$. We also measured the phase-matched third-harmonic generation from samples with different thickness. The third-harmonic intensities were indeed proportional to the square of the sample thickness.

Consider next the phase-matching conditions $3k_{-}^{(\omega)} = \bar{k}_{+}^{(3\omega)}$ and $3k_{-}^{(\omega)} = \bar{k}_{-}^{(3\omega)}$ (#2 and #6 in Table II). The setup in Fig. 6 was used for the measurements. The samples had left-handed helical structure, and therefore, the incoming laser beam was left circularly polarized to feed efficiently into the "-" mode. The third-harmonic signals generated in the backward direction were detected. The experimental results are shown in Figs. 9 and 10. There indeed exist peaks at the predicted phase-matching temperatures. However, the widths of the peaks are several times broader than those of the theoretical phase-matching curves for a monochromatic input laser beam. This broadening is due mainly to the large spectral content of the laser, as will be discussed later. As a further confirmation of the theoretical predictions, we found, in the same temperature ranges, no phase-matching peak for third-harmonic generation in the forward direction,

and also no peak for backward third-harmonic generation if the fundamental was right circularly polarized. We also found that the phase-matched third-harmonic outputs were nearly left and right circularly polarized (a ratio larger than 10 between two circularly polarized components) for the two cases, as predicted by the theory. The intensities of the phase-matched third harmonic generated by these mode combinations relative to that of mode combination #12 are given in Table III.

To observe the phase matching conditions #1, #4, #8 in the Tables, it would require the forward propagating fundamental waves to be in both "+" and "-" modes. Then, the incoming laser beam would have to be nearly linearly polarized. Consequently, large third-harmonic background signals would be created by the various components along the optical path. Our attempts to observe the phase-matching peaks on top of the background in these cases were not successful.

The remaining phase-matching conditions in the Tables except #13—#15 require the simultaneous presence of fundamental waves propagating in opposite directions along the helical axis. This was accomplished in two ways. One method was to construct the sample cell with a front-surface mirror in contact with the back of the sample. Each mode-locked pulse reflected back from the mirror overlaps with itself in the sample. Alternatively, we put a movable mirror at a distance beyond the sample equal to the optical length of the laser cavity (see Fig. 7). Then, each mode-locked pulse reflected back by the mirror meets the next pulse in the train in the sample cell. Both methods yielded the same results. The samples all had left-handed helical

structure. Right and left circularly polarized light fed efficiently into "+" and "-" modes respectively. Note that the sense of circular polarization is reversed upon reflection from a mirror. If a $\lambda/4$ retardation plate is inserted in front of the mirror, then the backward propagating light has the same circular polarization as the incoming beam. According to theory, the third-harmonic output in all these cases should be nearly circularly polarized.

Figure 11 shows the observed phase-matching peak at the predicted temperature for the #11 phase-matching condition. This peak had a relatively weak intensity and was observed with a reflecting back on the sample cell. No polarization measurement was attempted.

In Fig. 12, the observed small peak at 31.2°C came from #10 and the large peak at 29.9°C from #7 as predicted. Although the phase-matching peaks of #8 and #9 should also appear at 29.9°C, they were not excited with the given laser polarizations. The large peak had a 30:1 ratio of right-to-left circular components as expected. When the retardation plate was inserted with the incoming beam right circularly polarized, #9 was excited and the same phase-matching peak was observed with a much smaller amplitude. The peak due to #8 was not observed as mentioned earlier.

The phase-matching peaks of #3, #4, and #5 should appear at the same temperature. With the incoming beam left circularly polarized and without the $\lambda/4$ retardation plate in position, only #3 was excited. The observed phase matching peak shown in Fig.13 appeared at the predicted temperature. Also as predicted, the third harmonic was

generated only in the backward direction and had a 10:1 polarization ratio between the right and left circular components. With the retardation plate inserted, #5 was excited and the same phase matching peak was observed with a smaller amplitude. The third-harmonic output was nearly left circularly polarized as predicted. For reasons mentioned earlier, the peak due to #4 was not observed.

For the above cases, we also verified the necessity for the simultaneous presence of laser light propagating both forward and backward in order to generate phase-matched third harmonic radiation. By translating the movable mirror over a distance larger than 1 mm forward or backward from the position of maximum output, we essentially reduced the third-harmonic signal to zero. From such measurements, we could also deduce the pulsewidth of the mode-locked pulses (see Section V). In Table III, the peak intensities of the various phase-matching peaks relative to that of #12 are listed. In all these cases, the observed phase-matching peaks were much broader than the theoretical predictions assuming a monochromatic pump beam. The broadening was due to the broad spectral content of the mode-locked pulses, as we shall discuss in the next section.

The phase-matching conditions #13 and #14 cannot be satisfied in the liquid crystalline materials we used, but #15 can probably be satisfied at $p \sim 50$ μm in the mixture used to observe phase matching of #12. Our experimental effort to detect such a phase-matching peak was largely frustrated because the sample quality deteriorated when the pitch became large,[23,29] and because the large third-harmonic background generated from other components could not be eliminated in

this case.

V. DISCUSSION

We have seen in the previous section that the experimental results agree very well with the theoretical predictions in Section III. Therefore, this confirms the model of Oseen and de Vries[10,11] which assumes that optically, a cholesteric liquid crystal can be treated as a twisted birefringent medium.

If the overall molecular arrangement in planes perpendicular to the helical axis has no inversion symmetry, then second harmonic generation would be possible in a cholesteric liquid crystal, and would also be phase-matchable. The phase-matching condition $2k_+^{(\omega)} = k_+^{(2\omega)}$ would be satisfied at $p = 28$ μm in the mixture used to observe the phase-matched third-harmonic generation #12. Experimentally, we observed no second-harmonic phase-matching peak, suggesting that the contrary is true. Durand and Lee[7] and Goldberg and Schnur[8,9] have also found no second-harmonic generation in liquid crystals and have come to the same conclusion.

We notice that all the observed phase-matching peaks had widths greater than those predicted theoretically for a monochromatic laser and a perfect liquid crystal sample. In the latter case, the full width at half maximum of a phase matching peak in terms of pitch variation would be given by

$$\delta p_1 \simeq \frac{\pi}{L \frac{d(\Delta k)}{dp}} \tag{29}$$

where L is the sample thickness and d(Δk/)dp is the derivative of the phase mismatch Δk evaluated at Δk = 0. The value of $(\delta p)_1/p$ for each phase-matching peak is given in Table IV.

Surface effects on a liquid crystal sample are usually important. The molecular orientation on the boundary layers appears to remain unchanged despite changes in external parameters.[5,30] This constraint would not allow a perfect helical structure of arbitrary pitch to fit between the two interfaces. There would in general be a distortion of the helical structure amounting to ~ p/2 over the sample thickness. This implies a pitch distribution with a width $\delta p_2/p \sim p/2L$, the values of which at phase matching are given in Table IV. For the same sample thickness, this effect clearly increases with pitch, and appears to be a strong contribution to the observed width of the #12 phase matching peak occurring at $|p| \cong 17$ μm. There, in terms of temperature, the two widths corresponding to δp_1 and δp_2 are 0.2°C and 0.1°C respectively. The observed full width at half maximum is 0.3°C.

That the mode-locked pulses are far from being monochromatic would also introduce broadening in the phase matching peaks. The different frequency components of the laser pulses yield phase-matched third-harmonic (or more generally, sum-frequency) generation at different pitches. By assuming a spectral content of the mode-locked laser pulses of about 150 Å (full width at half maximum of a Gaussian pulse), presumably due mainly to frequency chirping, we obtain

convolution a width $\delta p_3/p = 7.5 \times 10^{-3}$ for all the phase-matching peaks. This value agrees quite well with the observed widths for all cases except #12 as indicated in Table IV, and therefore, the spectral content of the laser pulses is believed to be the dominant contribution for these cases.

As we mentioned earlier, our samples were actually composed of many domains with different orientations of the helical axis spread over a cone of about 12°. This might lead to additional broadening of the observed phase-matching peaks, since different domains would be at phase matching at different pitches if we allow the third-harmonic to be non-collinear with the fundamental. However, this effect would be small if the collection angle of the third-harmonic detector is small. In our experiments, the third-harmonic detector aligned with the beam had an acceptance angle of ~ 3°. The laser beam at the sample, even when it was focused, had a convergence angle less than 1°. This would contribute a width $\delta p_4/p$ to the phase-matching peak. The estimated values of $\delta p_4/p$ for the various cases are given in Table IV. They appear to be always less than the observed widths. In all cases except #12, there is a loss of third-harmonic power due to the fact that only domains with helical axes tipped at an angle less than 0.8° to 2.3° contribute to the observed third-harmonic. Compared to a perfect sample, this loss should be roughly a factor of 3 to 6.

From our measurements of the relative intensities of the various phase-matching peaks, we can deduce through Eq. (24) in the phase-matching approximation, the non-linear susceptibility elements C_{11}, C_{12}, C_{21}, and C_{22}, assuming that they are the same for different

mixtures. Using the measured intensities for the phase-matching peaks #2, #3, #6, #7, #11, and #12 (corrected for their different widths), we found from computer calculations that all four C's are nearly equal. Uncertainties in their values were large and came mainly from our relative intensity measurements. Because of the necessarily different experimental arrangement for the various phase-matching cases, correction for the differences introduced uncertainties. Different experimental runs also yielded slightly different results, presumably due to differences in sample quality. Taking all these factors into consideration, we can only conclude that C_{11}, C_{12}, C_{21}, and C_{22} are equal to within 10% and their values are uncertain within a factor of 2. Comparison with the third harmonic intensity generated in a phase-matched solution (45 gm/liter) of fuchsin dye in hexafluoracetone sesquihydrate[2] gave $|C/\chi^{NL}_{dye}| \sim 0.2$. This value could increase by a factor of 2 if the liquid crystal sample were of a single domain.

We realize that if C's are equal, then $\underset{\approx}{\chi}^{(3)}$ would be independent of z even in the lab frame. We can then find the solution of third-harmonic generation directly in the lab frame using Eq. (16). The optical fields in the equation can be written from Eq. (8) as

$$\underset{\sim}{E}_{\pm}(z,\omega) = [(\hat{x}+i\hat{y})A_{R\pm} \exp(i\omega n_{R\pm} z/C) + (\hat{x} - i\hat{y})A_{L\pm} \exp(i\omega n_{L\pm} z/C)]$$

$$\times (\mathcal{E}_{\xi\pm}/\sqrt{2}) \exp(-i\omega t). \qquad (30)$$

Phase-matched third harmonic generations should occur when individual components of $\underset{\sim}{E}_{\pm}$ are phase-matched, and the corresponding intensities

can be calculated knowing $A_{R\pm}^{(\omega)}$ and $A_{L\pm}^{(\omega)}$. For example, we have phase matching when

$$2n_{R+}^{(\omega)} + n_{L+}^{(\omega)} = 3n_{R+}^{(3\omega)}$$

or

$$2n_{L+}^{(\omega)} + n_{R+}^{(\omega)} = 3n_{L+}^{(3\omega)}$$

which can be easily shown to be equivalent to the phase matching condition #12. The corresponding third-harmonic field has $A_{R+}^{(3\omega)} \propto A_{R+}^{(\omega)} A_{R+}^{(\omega)} A_{L+}^{(\omega)}$ and $A_{L+}^{(3\omega)} \propto A_{L+}^{(\omega)} A_{L+}^{(\omega)} A_{R+}^{(\omega)}$. The relative intensities of the various phase-matching peaks calculated this way agree moderately well with the experimental results except for #2, #6, and #11 where the predicted intensities depend more critically on the inequality of the C's.

With C's being equal, the expected intensity of the phase-matching peak #10 should be four times greater than that of #7. However, our experimental data show that #10 is only 1/10 as intense as #7, or about 40 times weaker than predicted. The discrepancy is due to strong reflection of left-circularly polarized laser light from the sample, since the laser frequency is close to the reflection band of the sample. Measurements of transmission through the sample showed that only 1/10 of the left-circularly-polarized light was transmitted. Since this phase-matching case involves two left circularly-polarized fundamental fields (and one right), the strong reflection would decrease the observed third-harmonic intensity by a factor of 10^{-2}, assuming that the 90% reflection happens at the interface.

Phase-matched third-harmonic generation would of course occur in any cholesteric liquid crystal as long as the helical pitch can be adjusted to the correct value. We tried the experiment on an entirely different

cholesteric material. Poly-γ-benzyl-L-glutamate (PBLG), a synthetic α-helix protein, dissolved in dioxane is cholesteric for concentrations from ~ 0.1 gm to ~ 0.5 gm of PBLG per gm of solvent.[31] The dielectric constants are comparable to those of the cholesterol-derived materials and hence the pitches for phase-matching are approximately the same. A pitch of ~ 17 μm is realizable by adjusting the concentration of PBLG, and hence phase-matched third-harmonic generation #12 should be possible. We did not use temperature to tune the pitch because of the slow response of PBLG samples. Instead, we used many samples with different concentrations to yield different pitches. We did observe a peak in the third-harmonic intensity around p - 17 μm with the laser beam polarized to feed efficiently into the "+" mode, and no peak for the opposite laser polarization. There was a moderate amount of scattering in the data, presumably due to the use of many different samples.

Recently, measurements of ultrashort pulses have attracted much attention.[26,32-34] In all cases, except the case of Treacy using the compression technique,[33] the experiments measure only the pulse width. Both the second-harmonic generation technique and the two-photon fluorescence technique are inherently symmetric. They measure the auto correlation function $G^{(2)}(\tau) = \int |E(t)|^2 |E(t+\tau)|^2 dt$, which is characterized by $G^{(2)}(\tau) = G^{(2)}(-\tau)$, and therefore cannot yield any information about the pulse shape. Phase-matched third-harmonic generation has also been used for pulse-width measurements,[34] but only under circumstances where a symmetrized form of the third-order auto-correlation function was observed. Here, in principle, the technique

can provide information about the pulse width as well as pulse asymmetry. If phase matching requires two fundamental photons in one mode and one in the other mode, then we can measure the correlation function $G^{(3)}(\tau) = \int_{-\infty}^{\infty} |E(t)|^4 |E(t+\tau)|^2 \, dt \neq G^{(3)}(-\tau)$. This correlation function is symmetric ($G(\tau) = G(-\tau)$) only if the pulse is symmetric. Therefore, from the asymmetry of $G(\tau)$, we can deduce information about the pulse asymmetry.[4,35] Most of the phase-matching conditions in cholesteric liquid crystals satisfy this requirement.

To demonstrate the technique, we split the laser beam into two beams with proper polarizations to excite the phase-matching peak #7. The two beams, after traveling about the same optical path, met each other at the sample from opposite sides. A variable optical delay in one arm allowed continuous variation of the relative arrival time τ of the two pulses. Our results are shown in Fig. 14. The curve shows an average pulse width of about 7.5 psec and a pulse asymmetry in the sense that the trailing edge of the pulse was steeper than the leading edge. This agrees with the result of Treacy.[33] Assuming an asymmetric pulse constructed from two half Gaussian curves joined at their maxima, with their widths differed by a factor of 5.5, we obtained a correlation curve which fits well with the data, as shown in Fig. 14. However, this curve is not very sensitive to the pulse asymmetry.[35] Consequently, unless the third-harmonic generation can be measured very accurately, the technique cannot yield very good quantitative measure of the pulse asymmetry. Prior knowledge of the pulse shape would also be necessary for more accurate conclusion. Since better signal-to-noise ratio would help the resolution, we should

probably use crystals such as calcite as the nonlinear medium in such measurements, where phase-matched third-harmonic generation can be achieved with two fundamental photons in the ordinary mode and one in the extraordinary mode.[36] There, with the fundamental and the third-harmonic propagating in the same direction, the signals can be much stronger. Ideally, one would like to obtain information about the pulse asymmetry for individual pulses instead of averages over all the pulses in a train.

Our maximum observed energy conversion from the laser frequency to the third-harmonic was small. The most efficient case was #12. Without focusing, the 130 μm thick samples converted about 10^{-14} of the laser energy to the third harmonic. By focusing the laser beam down to 0.1 mm diameter, we could increase the conversion by a factor of $\sim 4 \times 10^2$. Although thicker samples of good quality could probably be made with the help of external fields, the conversion efficiency would still be too small for such samples to be useful as practical third-harmonic generators.

We can of course also have other types of nonlinear interaction phase-matched in a cholesteric liquid crystal. We realize that it is the periodicity of the medium which makes phase matching easily achievable here. It is clear that other media with periodicity in the optical range can also be used. In fact, our theoretical analysis in Sections II and III, using the Bloch picture should be applicable to all such materials. Bloembergen and Sievers have considered possibilities for phase matching of a number of nonlinear interactions in periodic layers of GaP and GaAs.[37] This layer medium lacks inversion

symmetry, thus permitting the observation of second-order non-linear effects. However, it is difficult to fabricate and not so directly tunable. The great advantage of cholesteric liquid crystals is their inherent and variable periodicity.

VI. CONCLUSIONS

We have shown theoretically and experimentally that third-harmonic generation can be collinearly phase-matched in cholesteric liquid crystals. Phase-matching is achieved since the momentum mismatch between the fundamental and the third harmonic is compensated by the lattice momentum which is present due to the periodicity of the helical structure of the cholesteric medium. Many different phase-matching conditions exist. Analogous to electron-electron interaction in a periodic lattice, they can be identified as normal and umklapp processes respectively. Most of the predicted phase-matching conditions were confirmed experimentally. In several cases, phase-matched third-harmonic generation occurs only when the fundamental waves appear simultaneously propagating in opposite directions. These processes can be used to measure the width and asymmetry of the mode-locked pulses. We also attempted to observe second-harmonic generation in cholesteric liquid crystals. The negative results indicate that the molecular arrangement of the liquid crystals in a plane perpendicular to the helical axis has an overall inversion symmetry. The theoretical discussion in this paper can be extended to other types of media with periodicity in the optical range.

ACKNOWLEDGEMENTS

This work was performed under the auspices of the U. S. Atomic Energy Commission.

REFERENCES

* Permanent Address: Phys. Dept., Williams College, Williamstown, Mass.

1. J. Giordmaine, Phys. Rev. Letters 8, 19 (1962); P. D. Maker, R. W. Terhune, M. Nisenoff, and C. M. Savage, Phys. Rev. Letters 8, 21 (1962).
2. H. Rabin and P. P. Bey, Phys. Rev. 156, 1010 (1967); C. K. N. Patel and N. Van Tran, Appl. Phys. Letters 15, 189 (1969).
3. J. P. Bey, J. F. Guiliani, and H. Rabin, Phys. Rev. Letters 19, 819 (1967); R. K. Chang and L. K. Galbraith, Phys. Rev. 171, 993 (1968).
4. J. W. Shelton and Y. R. Shen, Phys. Rev. Letters 25, 23 (1970); 26, 538 (1971).
5. See, for example, G. W. Gray, Molecular Structure and the Properties of Liquid Crystals (Academic, New York, 1962); I. G. Chistyakov, Soviet Physics Uspekhi 9, 551 (1967); G. H. Brown, J. W. Doane, and V. D. Neff, CRC Critical Reviews in Solid State Sciences 1, 303 (1970).
6. I. Freund and P. M. Rentzepis, Phys. Rev. Letters 18, 393 (1967).
7. G. Durand and C. H. Lee, Molecular Crystals 5, 171 (1968).
8. L. S. Goldberg and J. S. Schnur, Appl. Phys. Letters 14, 306 (1969).
9. L. S. Goldberg and J. S. Schnur, Radio Electronic Engr. (GB) 39, 279 (1970).
10. C. W. Oseen, Trans. Faraday Soc. 29, 883 (1933).
11. H. de Vries, Acta Cryst. 4, 219 (1951).
12. I. Freund, Phys. Rev. Letters 21, 1404 (1968).
13. See, for example, C. Kittel, Introduction to Solid State Physics (J. Wiley, New York, 1966), 3d ed.

14. D. W. Berreman and T. J. Scheffer, Molecular Crystals and Liquids Crystals 11, 395 (1970); D. Dreher, G. Meier, and A. Saupe, Molecular Crystals and Liquid Crystals 13, 17 (1971).

15. See, for example, C. P. Slichter, Principles of Magnetic Resonance (Harper & Row, New York, 1963), p. 11.

16. See, for example, N. Bloembergen, Nonlinear Optics (Benjamin, 1964).

17. P. N. Butcher, Nonlinear Optical Phenomena (Ohio State University Engineering Publications, 1965).

18. As long as the field variation across the beam profile is not too rapid, we can use ray approximation fo find $|\mathcal{E}_{\pm}(3\omega,x,y)|^2$ at local points.

19. H. J. Simon and N. Bloembergen, Phys. Rev. 171, 1104 (1968); C. L. Tang and H. Rabin, Phys. Rev. B3, 4025 (1971).

20. These chemicals were obtained from Aldrich Chemical Co., Eastman Organic Chemicals, and Varilight Corporation, and were used without further purification.

21. For more information on this three-component cholesteric system see: J. L. Fergason, Appl. Optics 7, 1729 (1968); J. L. Fergason, Am. J. of Physics 38, 425 (1970); L. Melamed and D. Rubin, Appl. Optics 10, 1103 (1971).

22. See, for example, F. W. Sears, Optics (Addison-Wesley, Reading, Mass., 1949), p. 47.

23. H. Baessler, T. M. Laronge, and M. M. Labes, J. Chem. Phys. 51, 3213 (1969).

24. C. Robinson, Tetrahedron 13, 219 (1961).

25. E. Sackmann, S. Meiboom, L. C. Snyder, A. E. Meixner, and R. E. Dietz, J. Am. Chem. Soc. 90, 3567 (1968).

26. J. A. Giordmaine, P. M. Rentzepis, S. L. Shapiro, and K. W. Wecht, Appl. Phys. Letters 11, 216 (1967).

27. P. P. Bey and H. Rabin, Phys. Rev. 162, 794 (1967).

28. J. Ducuing and N. Bloembergen, Phys. Rev. 133, 1493 (1964).

29. P. Kassubek and G. Meier, Molecular Crystals and Liquid Crystals 8, 305 (1969).

30. P. Chatelain, Bull. Soc. Franc. Mineral. Crist. 66, 105 (1943).

31. C. Robinson, J. C. Ward, and R. B. Beevers, Disc. Faraday Soc. 25, 29 (1958).

32. J. A. Armstrong, Appl. Phys. Letters 10, 16 (1967).

33. E. B. Treacy, Appl. Phys. Letters 14, 112 (1969).

34. R. C. Eckardt and C. H. Lee, Appl. Phys. Letters 15, 425 (1969).

35. H. P. Weber and R. Dandliker, Phys. Letters 28A, 77 (1968).

36. P. D. Maker and R. W. Terhund, Phys. Rev. 137, A801 (1965).

37. N. Bloembergen and A. J. Sievers, Appl. Phys. Letters 17, 483 (1970).

FIGURE CAPTIONS

Fig. 1. Relative amplitude of the two circularly polarized components of the two propagating modes in the lab frame as a function of the reduced wavelength. Here, $\alpha = 0.03$ and the helical structure is assumed right-handed. For a left-hand structure, the ratios are inverted.

Fig. 2. Polarization of the normally incident light which feeds exclusively into the two propagating modes in a left-handed cholesteric medium with $\alpha = 0.03$ and $\bar{\varepsilon} = 2.25$. Curves 1 and 2 are for "+" and "-" modes respectively. e_y/e_x indicates the ratio of the field components along $\hat{y}$ and $\hat{x}$.

Fig. 3. $(p\bar{\varepsilon}^{1/2})^{-1}$ as a function of the concentration of cholesteryl chloride in a mixture containing equal amounts of cholesteryl oleyl carbonate and cholesteryl nonanoate at 20°C and 40°C. A negative p indicates a left-handed cholesteric structure. Mixtures containing $\gtrsim$ 80% cholesteryl chloride are "super-cooled" liquid-crystal mixtures at these temperatures and are unstable. When freshly prepared, they last only for a few minutes before transforming to crystals.

Fig. 4. Variation of the birefringence factor α as a function of temperature at 6328 Å for the mixture of cholesteryl chloride and cholesteryl myristate (1.75:1 by weight). The solid curve is a smooth fit to the data points.

Fig. 5. Variation of the inverse pitch (1/p) with temperature for the mixture of cholesteryl chloride and cholesteryl myristate (1.75:1 by weight). The experimental uncertainty is $\pm$ 0.005 μm^{-1}. The solid curve is a smooth fit to the data points.

Fig. 6. Experimental arrangement for observing third-harmonic generation in cholesteric liquid crystals: LP (linear polarizer); GS (glass slide); LF (laser attentuation filter); L (lens); LQ (liquid crystalline sample); WB (water bath); IF (interference filter at 0.353 μm); IP21 (photomultiplier); $(1/4)\lambda$ (quarter-wave plate at 1.06 μm); FB (fuchsin dye cell). Corning and Schött glass filters are labeled by their catalog numbers.

Fig. 7. Experimental arrangement for observing phase-matched third-harmonic generation in cholesteric liquid crystals requiring the simultaneous presence of laser light propagating both forward and backward. The two optical paths marked "L" are equal to ensure overlapping of the pico-second mode-locked pulses in the sample. MM (movable mirror); RP (retardation plate); REF (reference arm for creating third-harmonic reference signals). The unlabeled optical components are the same as in Fig. 6.

Fig. 8. Phase-matching peaks for mode combination #12 observed with a sample 130 μm thick. The peak at the lower temperature is generated by right-circularly polarized fundamental waves and the one at the higher temperature by left-circularly polarized fundamental waves. The solid line is the theoretical phase-matching curve and the dots are experimental data points. The uncertainty in the experimental third-harmonic intensity is about 20%.

Fig. 9. Phase-matching peak for mode combination #2 observed with a sample 130 μm thick. The circles are experimental points with an uncertainty of 20%. The curve is a smooth fit to the data.

Fig. 10. Phase-matching peak for mode combination #6 observed with a sample 130 μm thick. The circles are the experimental data and have about a 20% uncertainty. The solid line is a theoretical phase-matching curve, assuming a spectral content of 150 Å for the laser pulses.

Fig. 11. Phase-matching peaks for mode combination #11 observed with a sample 130 μm thick. The circles are experimental points with an uncertainty of 20%. The curve is a smooth fit to the data.

Fig. 12. Phase-matching peak for mode combinations #7 and #10 observed with a sample 130 μm thick. The circles are experimental points with an uncertainty of 20%. The curve is a smooth fit to the data.

Fig. 13. Phase-matching peak for mode combination #3 observed with a sample 130 μm thick. The circles are experimental points with an uncertainty of about 20%. The curve is a smooth fit to the data.

Fig. 14. Normalized third-harmonic power vs relative time delay of the two fundamental laser pulses propagating in opposite directions in the mixture of Fig. 12 at the phase-matching temperature 29.9°C. The circles are experimental points with an uncertainty of 20%. The solid curve is obtained from theoretical calculation by assuming that the mode-locked pulses are made of two half Gaussian curves joined at their maxima, with the leading half 5.5 times broader than the lagging half.

TABLE CAPTIONS

Table I. Mode combinations for possible phase matching of harmonic generation assuming $\bar{\varepsilon}^{(3\omega)} > \bar{\varepsilon}^{(\omega)}$. The phase-matching conditions are expressed in terms of the average wave vectors using the approximation of Eq. (27) in the second column, and in terms of the wave vectors for Bloch wavefunctions in the third column. The superbars indicate backward propagating modes. For typical cholesteric materials with $\bar{\varepsilon}^{(\omega)} = 2.18$, $\bar{\varepsilon}(3\omega) = 2.30$, and $\alpha = 0.03$, the approximate pitches for the various phase matching cases are given in the last column.

Table II. Empirical data on the various cholesteric mixtures used to observe phase-matched third-harmonic generation. Predicted phase-matching pitches are calculated using Eqs. (6) and (26).

Table III. Predicted and observed phase-matching temperatures and relative third-harmonic peak intensities in various cases. dp/dT is the rate of change of pitch with temperature at the phase-matching temperatures. A negative pitch indicates a left-handed helical structure.

Table IV. Various possible contributions to the widths of the phase-matching peaks together with the predicted and the observed widths of the peaks. $d(\Delta k)/dp$ is the rate of change of the phase mismatch with pitch at phase matching. δp_1, δp_2, δp_3, and δp_4 for a sample 130 μm thick due respectively to the inherent width, the surface effect on helical structure, the spectral content of laser pulses, and the domain structure in the samples.

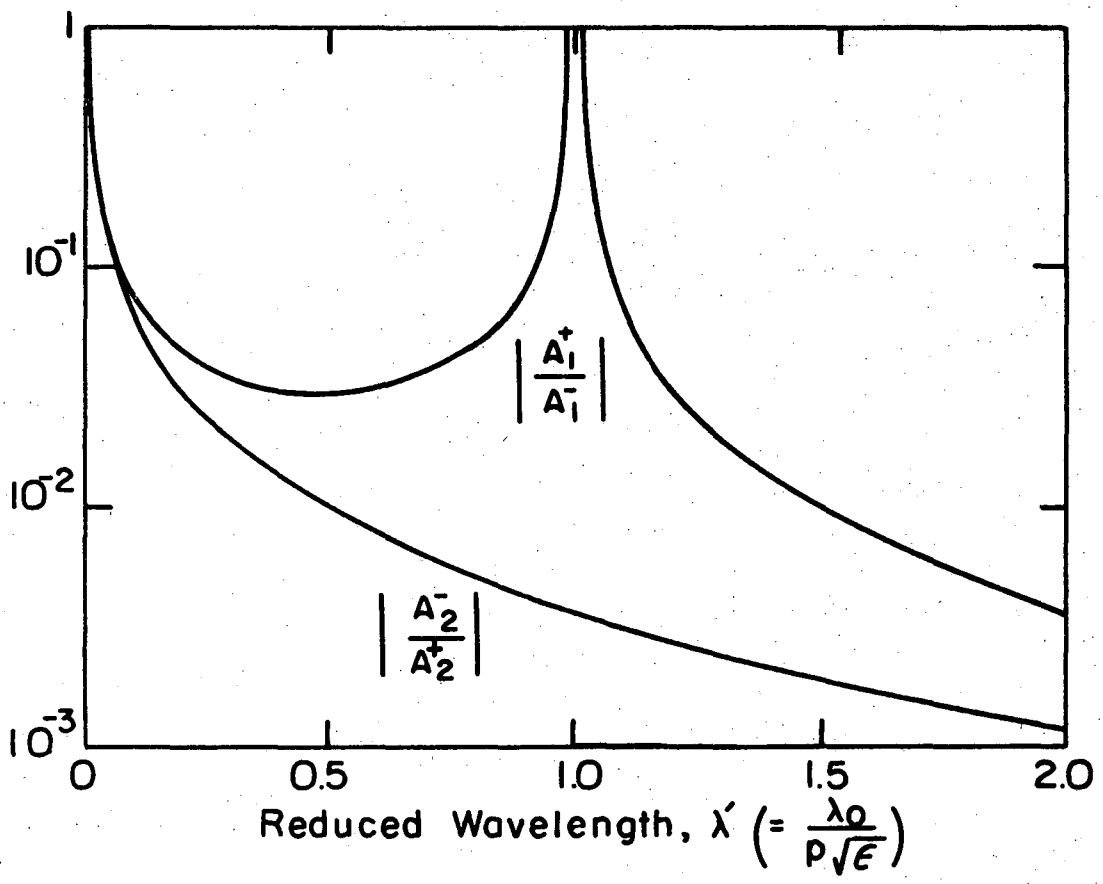

XBL 717-6958

Fig. 1

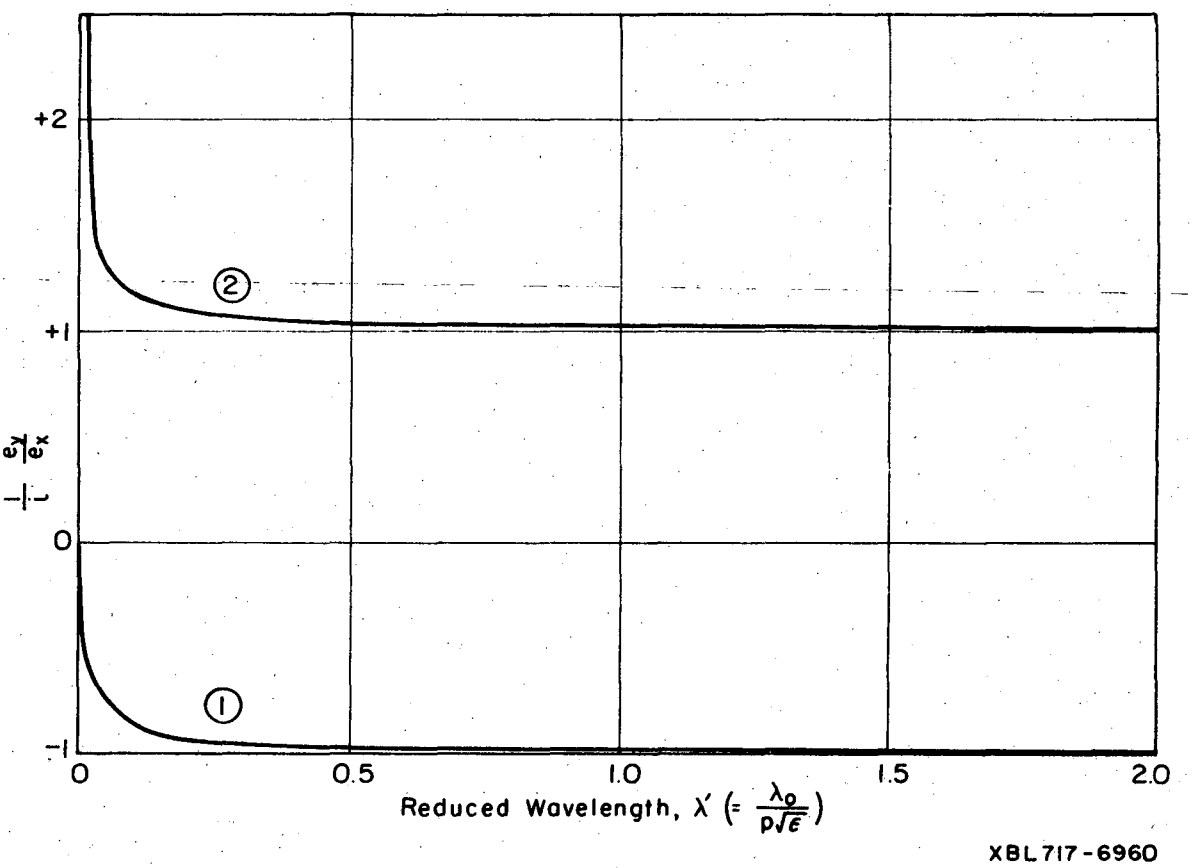
+2
+1
0
−1
$\frac{e_y}{e_x}$
①
②
0
0.5
1.0
1.5
2.0
Reduced Wavelength, $\lambda' \left(= \frac{\lambda_0}{p\sqrt{\epsilon}}\right)$
XBL717-6960

Fig. 2

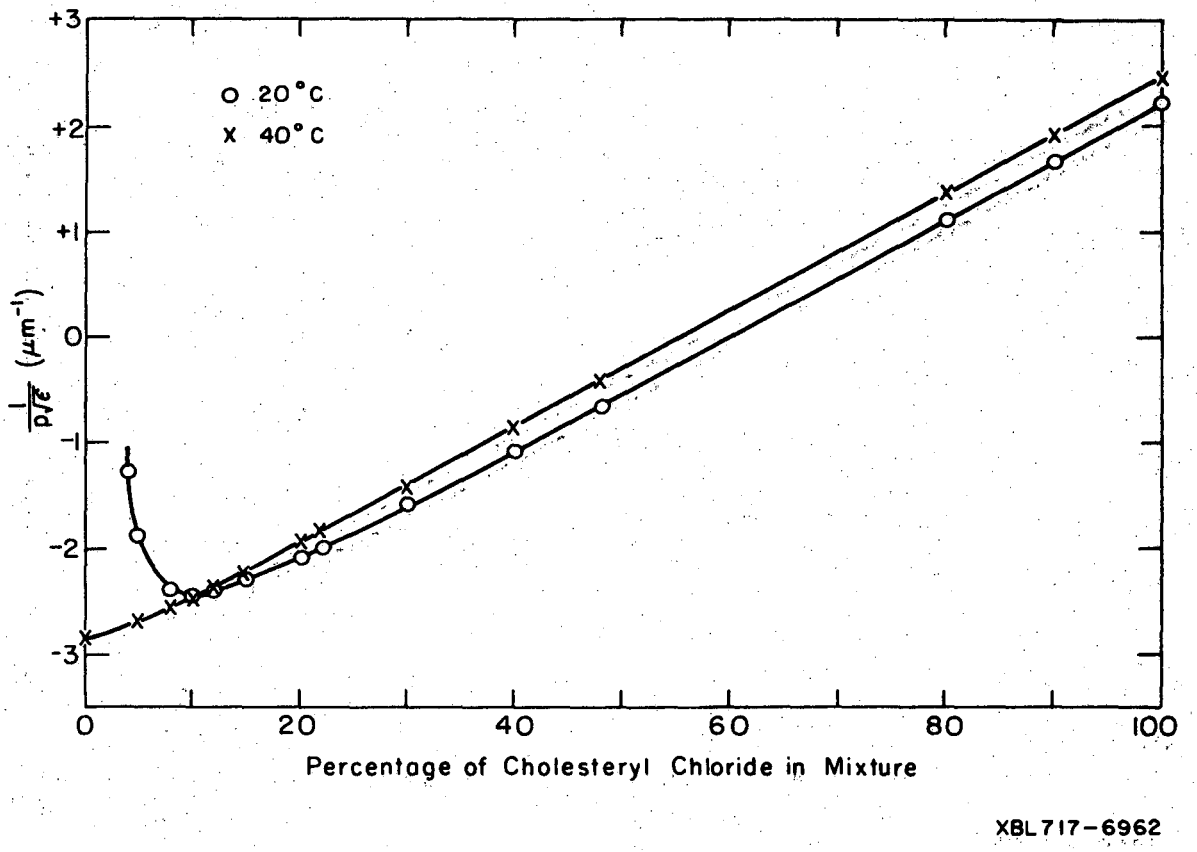
+3
+2
+1
0
-1
-2
-3
o 20°C
x 40°C
$\frac{1}{p/\ell}$ (μm^{-1})
0
20
40
60
80
100
Percentage of Cholesteryl Chloride in Mixture
XBL717-6962

Fig. 3

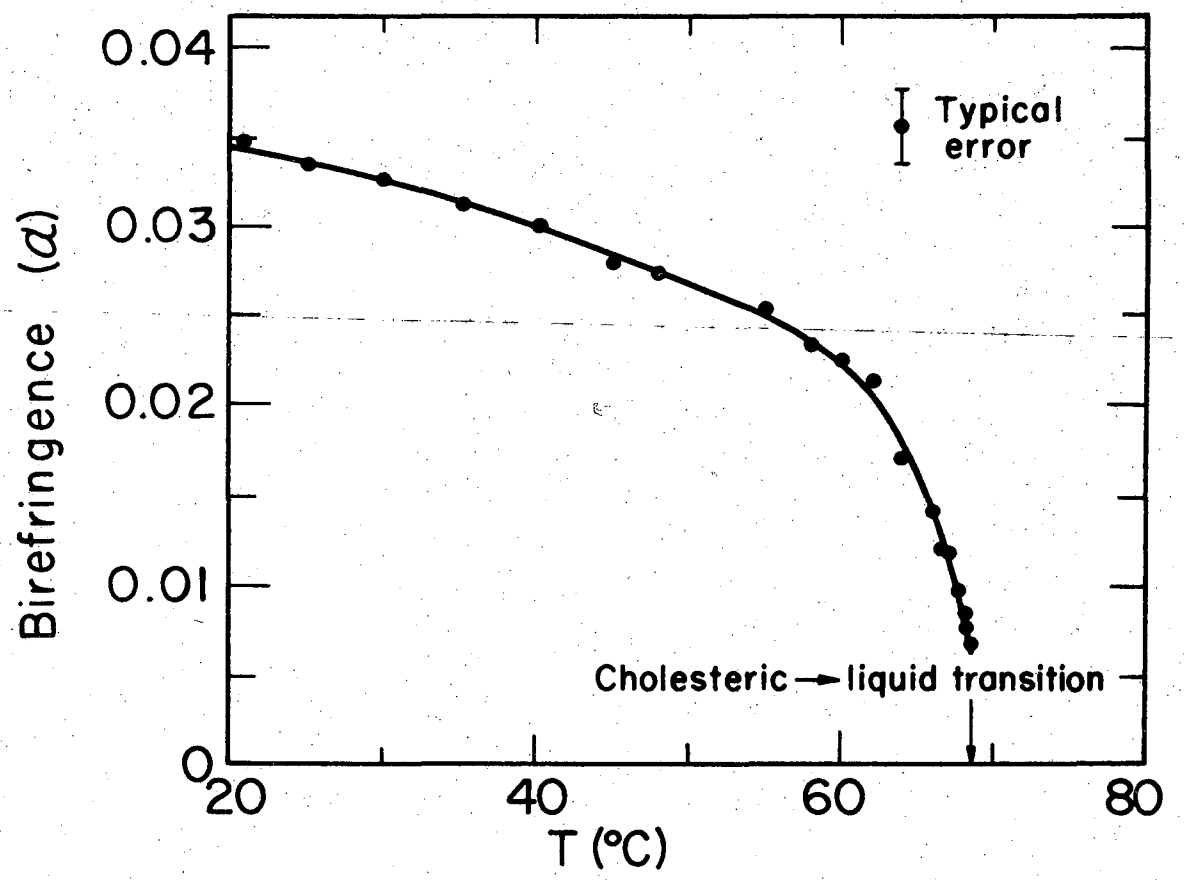
0.04
0.03
0.02
0.01
0
Birefringence (α)
Typical error
Cholesteric → liquid transition
20
40
60
80
T (°C)
XBL704-2691

Fig. 4

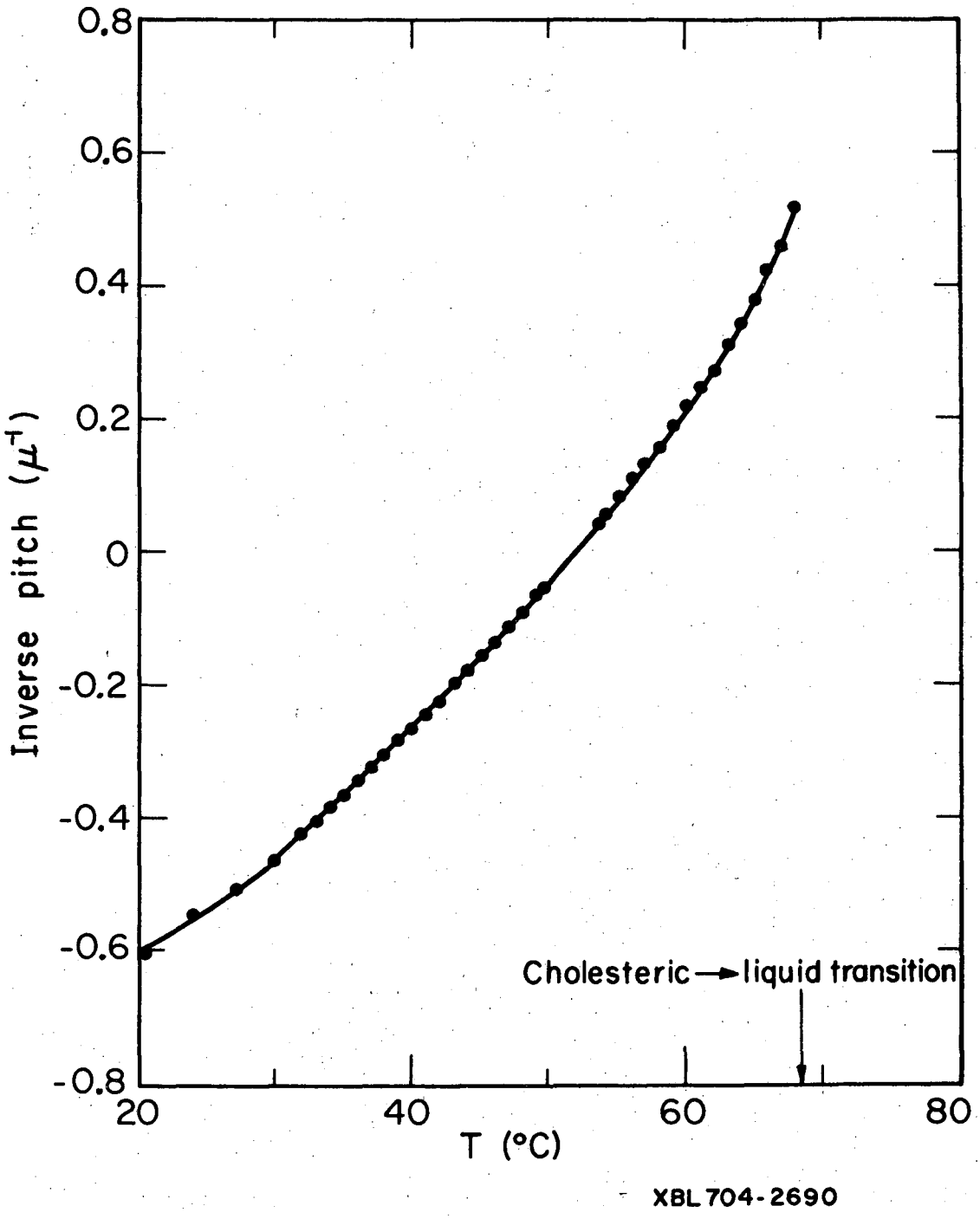
0.8
0.6
0.4
0.2
0
-0.2
-0.4
-0.6
-0.8
Inverse pitch (μ^{-1})
20
40
60
80
T (°C)
Cholesteric → liquid transition
XBL704-2690

Fig. 5

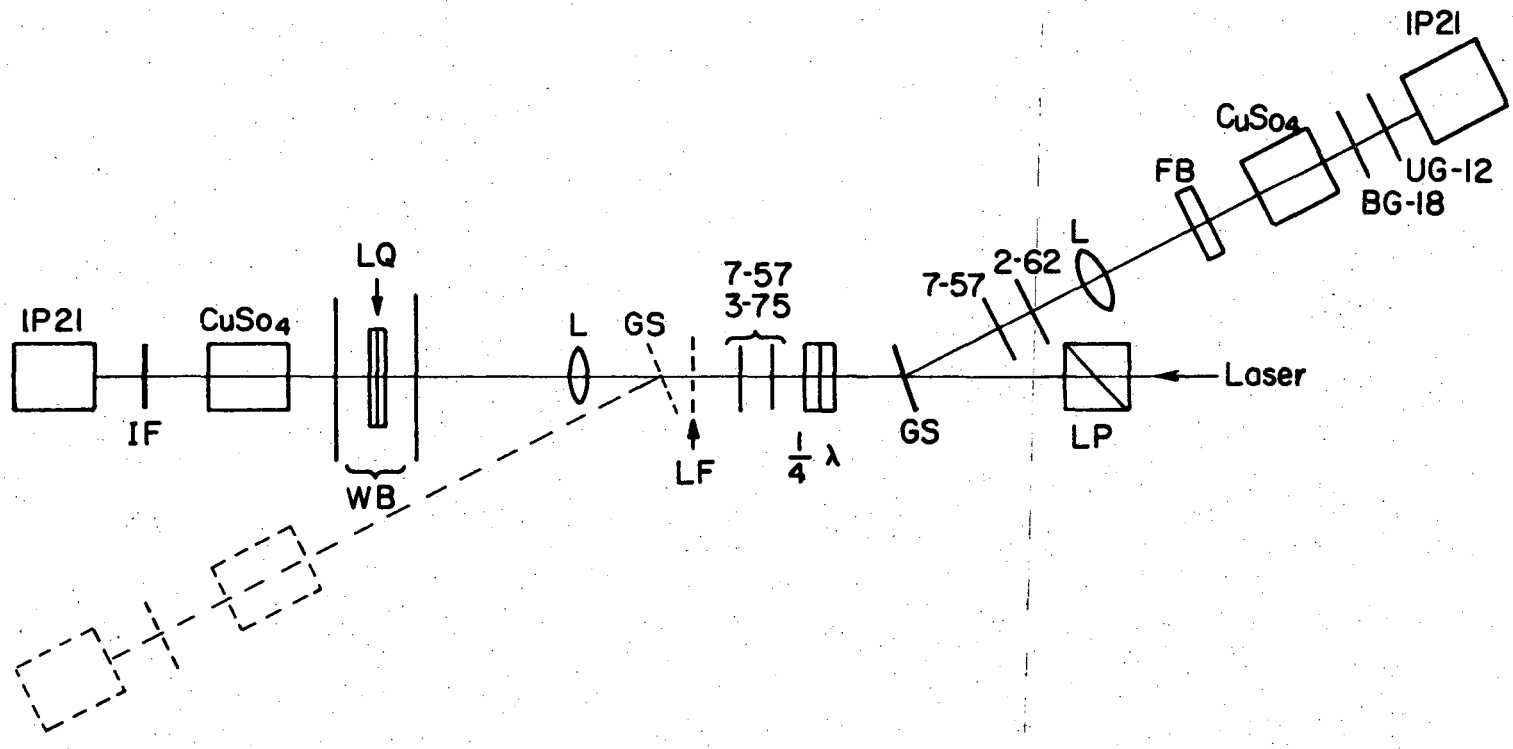

XBL 717-6963

Fig. 6

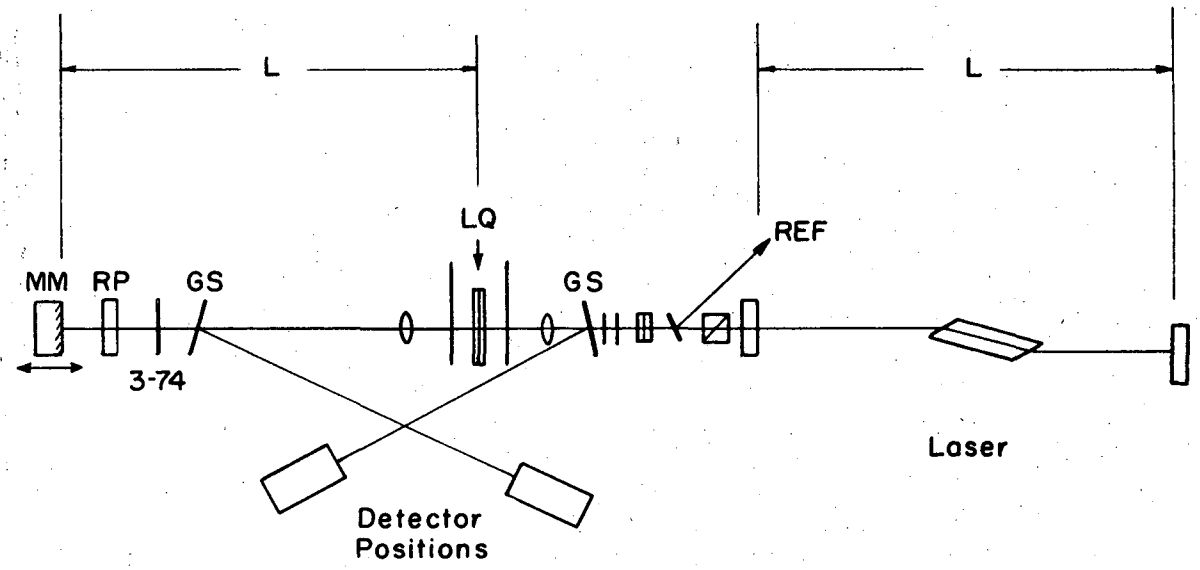
L
L
LQ
REF
MM
RP
GS
GS
3-74
Laser
Detector
Positions
XBL 717-6965

Fig. 7

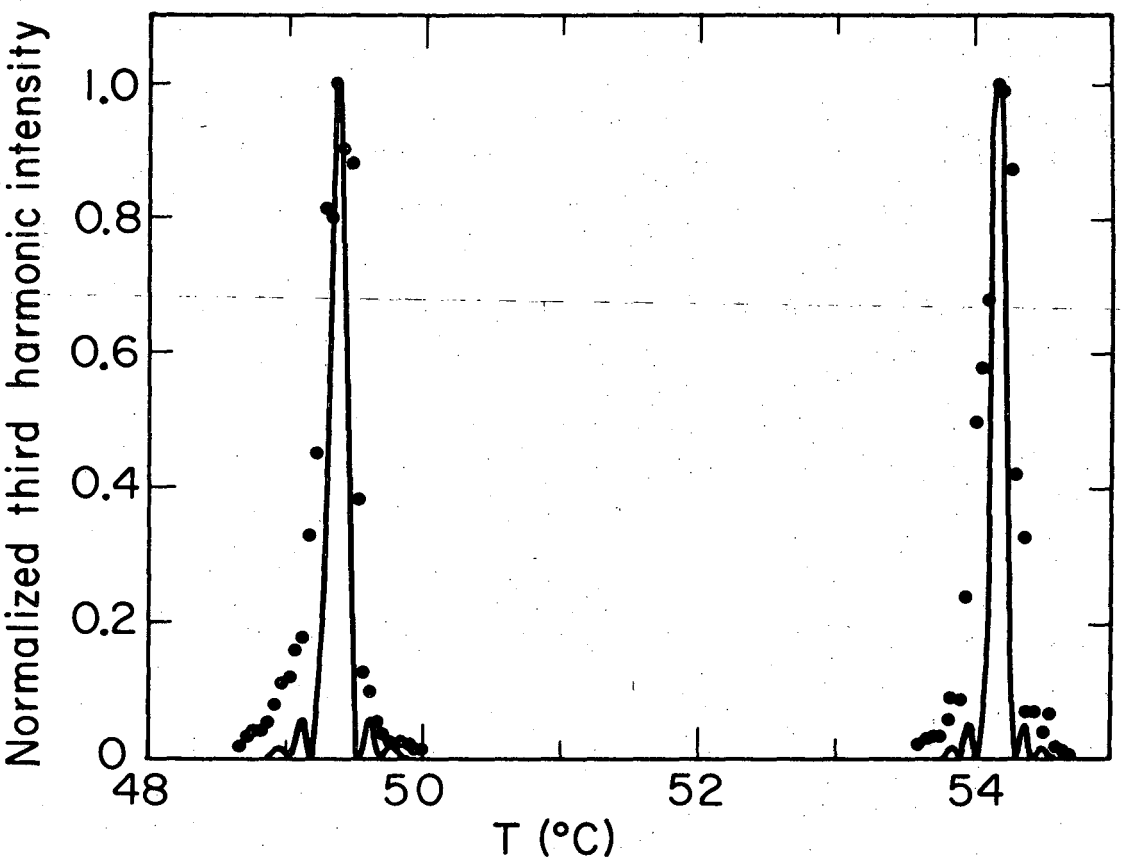
Normalized third harmonic intensity
1.0
0.8
0.6
0.4
0.2
0
48
50
52
54
T (°C)
XBL 704-2692

Fig. 8

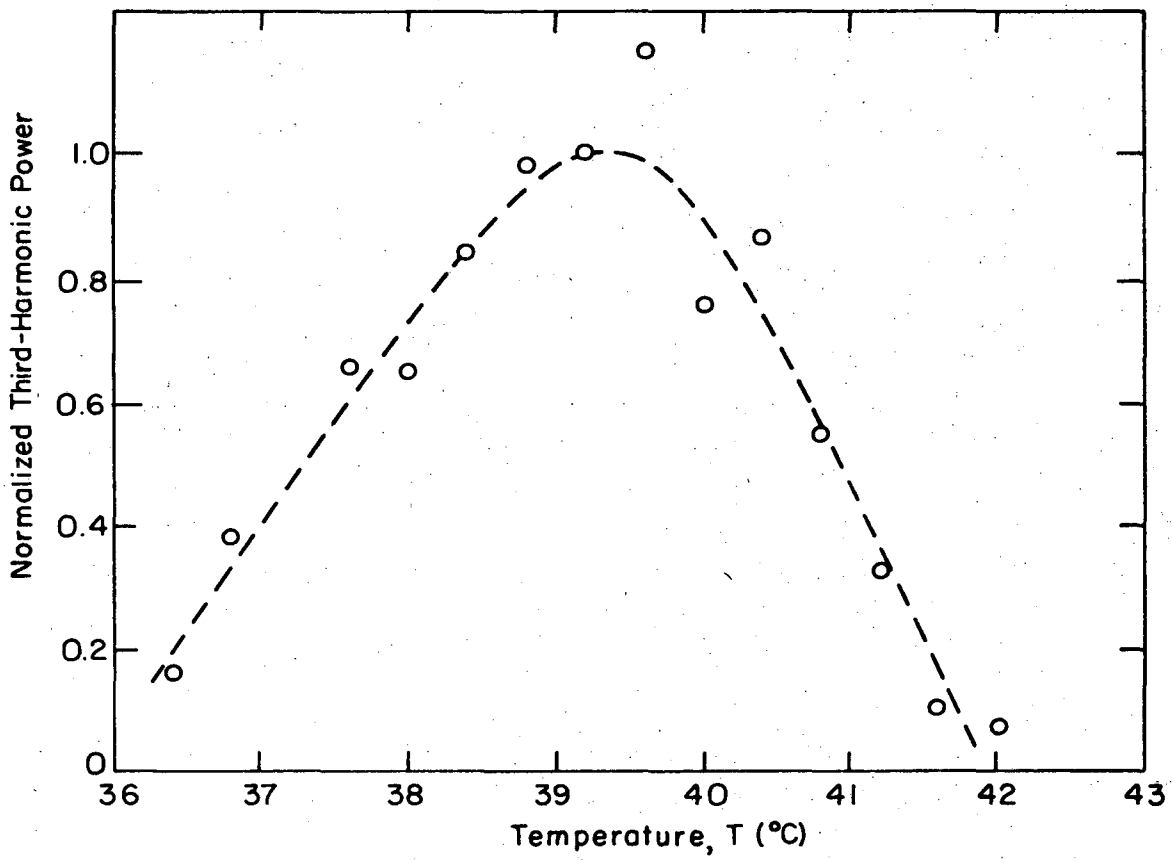

XBL 717-6964

Fig. 9

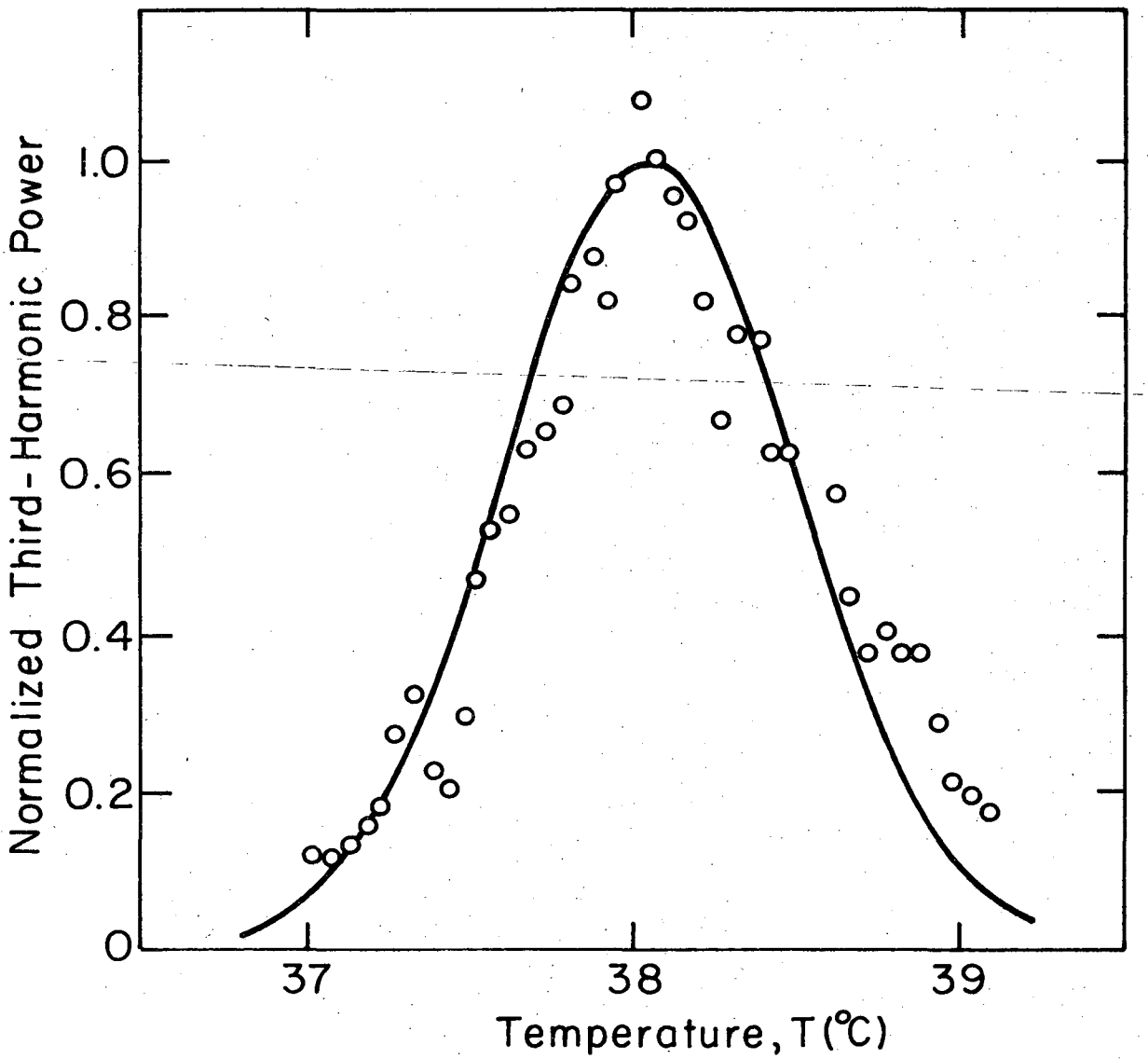

XBL 7012-7411

Fig. 10

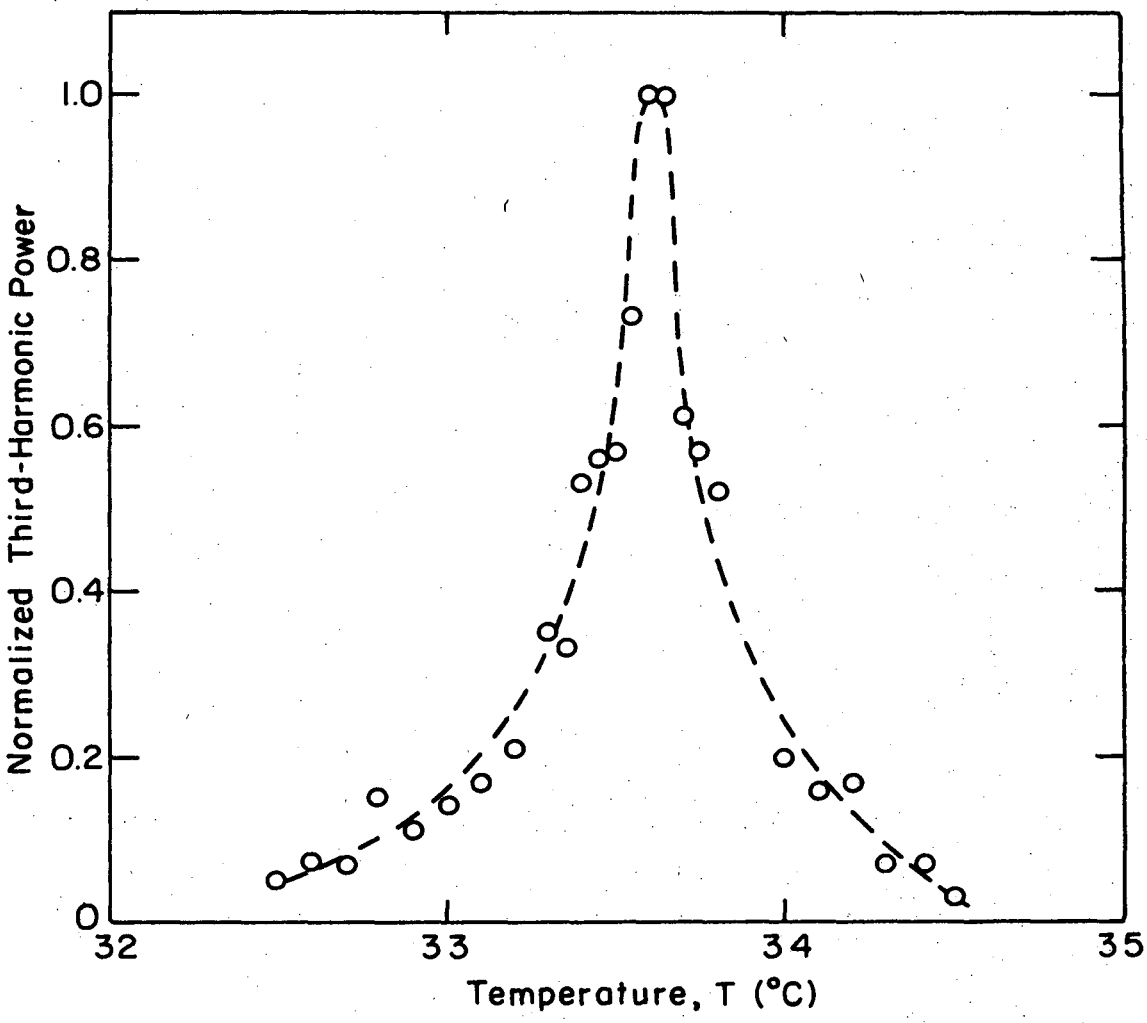

XBL717-6966

Fig. 11

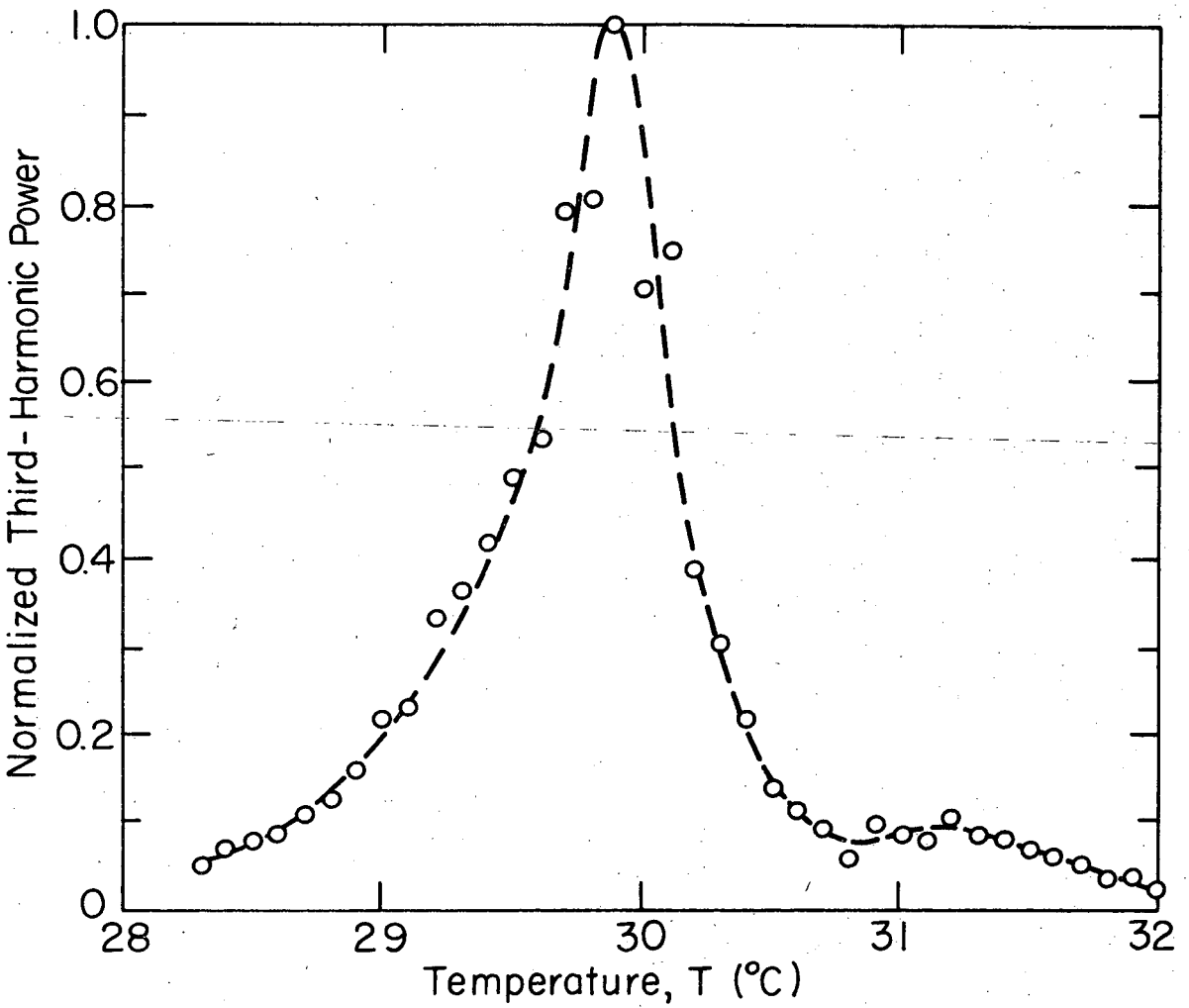

XBL 7012-7409

Fig. 12

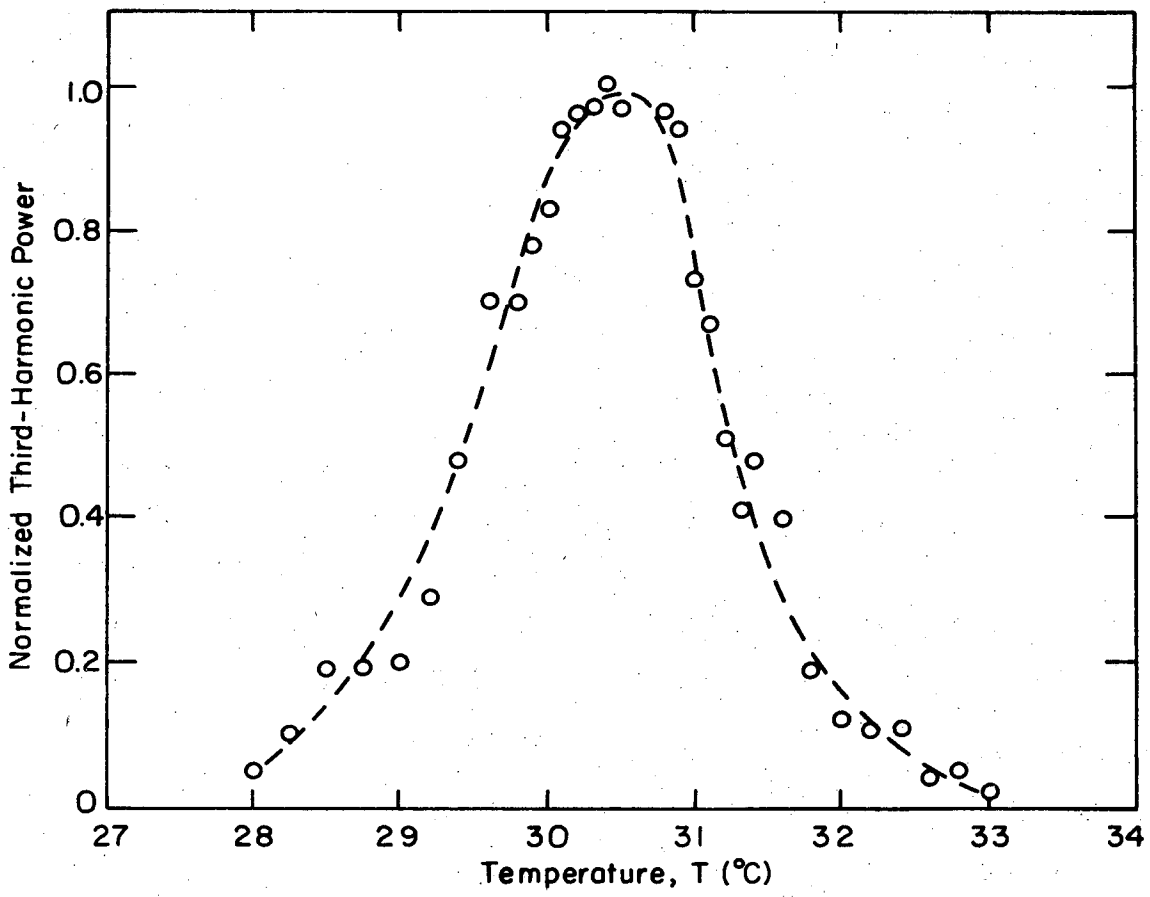

XBL717-6967

Fig. 13

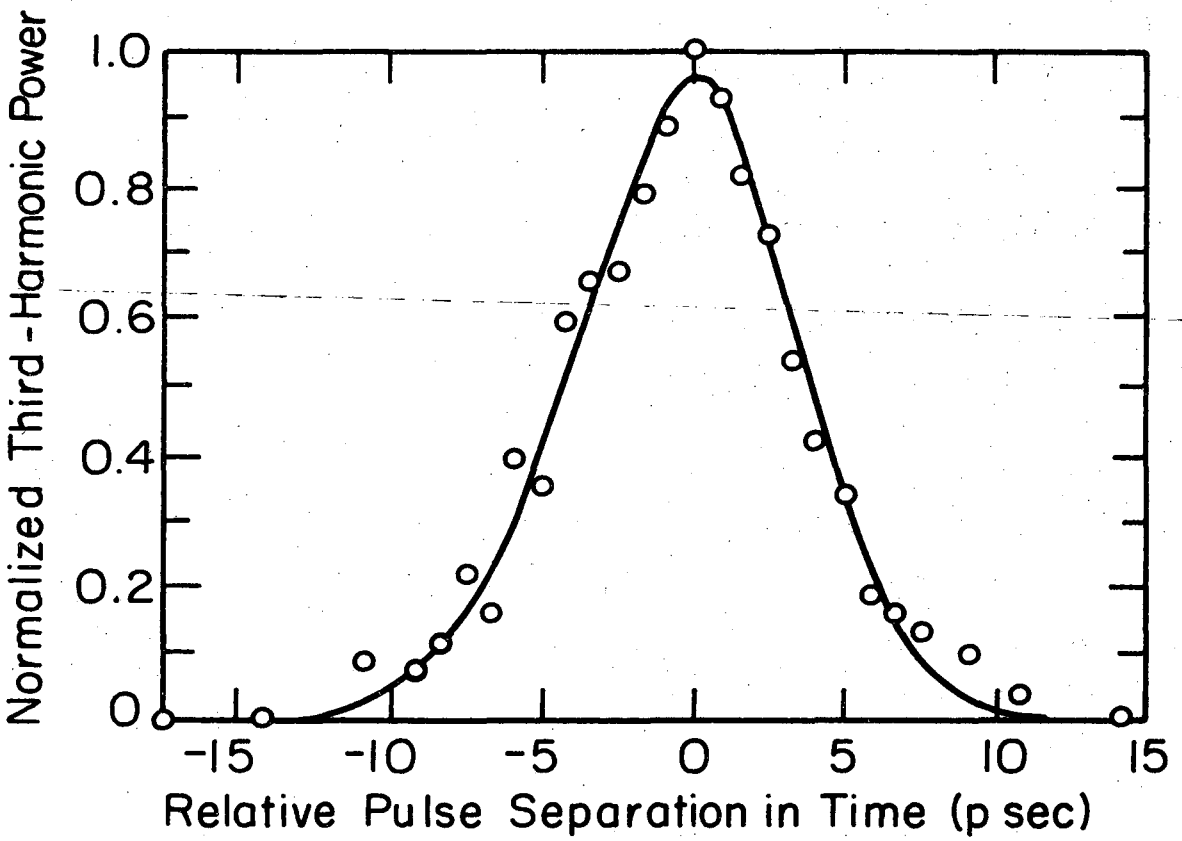

XBL 719-7219

Fig. 14

	Mode Combination for Phase Matching			Pitch for Phase Matching (μm)
1.	$k_+^{(\omega)}+2k_-^{(\omega)}=\bar{k}_-^{(3\omega)}$	$3k_o^{(\omega)}=\bar{k}_o^{(3\omega)}+Q$	$\kappa_+^{(\omega)}+2\kappa_-^{(\omega)}=\bar{\kappa}_-^{(3\omega)}$	0.24
2.	$3k_-^{(\omega)}=\bar{k}_+^{(3\omega)}$		$3\kappa_-^{(\omega)}=\bar{\kappa}_+^{(3\omega)}+Q$	0.24
3.	$\bar{k}_+^{(\omega)}+2k_-^{(\omega)}=\bar{k}_+^{(3\omega)}$		$\bar{\kappa}_+^{(\omega)}+2\kappa_-^{(\omega)}=\bar{\kappa}_+^{(3\omega)}$	0.35
4.	$k_+^{(\omega)}+\bar{k}_+^{(\omega)}+k_-^{(\omega)}=\bar{k}_-^{(3\omega)}$	$2k_o^{(\omega)}+\bar{k}_o^{(\omega)}=\bar{k}_o^{(3\omega)}+Q$	$\kappa_+^{(\omega)}+\kappa_-^{(\omega)}+\bar{\kappa}_+^{(\omega)}=\bar{\kappa}_-^{(3\omega)}$	0.35
5.	$2k_-^{(\omega)}+\bar{k}_-^{(\omega)}=\bar{k}_-^{(3\omega)}$		$2\kappa_-^{(\omega)}+\bar{\kappa}_-^{(\omega)}=\bar{\kappa}_-^{(3\omega)}$	0.35
6.	$3k_-^{(\omega)}=\bar{k}_-^{(3\omega)}$	$3k_o^{(\omega)}=\bar{k}_o^{(3\omega)}+2Q$	$3\kappa_-^{(\omega)}=\bar{\kappa}_-^{(3\omega)}+Q$	0.47
7.	$2k_+^{(\omega)}+\bar{k}_-^{(\omega)}=k_+^{(3\omega)}$		$2\kappa_+^{(\omega)}+\bar{\kappa}_-^{(\omega)}=\kappa_+^{(3\omega)}+Q$	0.69
8.	$k_+^{(\omega)}+k_-^{(\omega)}+\bar{k}_-^{(\omega)}=k_-^{(3\omega)}$	$2k_o^{(\omega)}+\bar{k}_o^{(\omega)}=k_o^{(3\omega)}-Q$	$\kappa_+^{(\omega)}+\kappa_-^{(\omega)}+\bar{\kappa}_-^{(\omega)}=\kappa_-^{(3\omega)}+Q$	0.69
9.	$2k_+^{(\omega)}+\bar{k}_+^{(\omega)}=k_-^{(3\omega)}$		$2\kappa_+^{(\omega)}+\bar{\kappa}_+^{(\omega)}=\kappa_-^{(3\omega)}+Q$	0.69
10.	$\bar{k}_+^{(\omega)}+2k_-^{(\omega)}=\bar{k}_-^{(3\omega)}$	$2k_o^{(\omega)}+\bar{k}_o^{(\omega)}=\bar{k}_o^{(3\omega)}+2Q$	$\bar{\kappa}_+^{(\omega)}+2\kappa_-^{(\omega)}=\bar{\kappa}_-^{(3\omega)}$	0.70
11.	$2k_+^{(\omega)}+\bar{k}_-^{(\omega)}=k_-^{(3\omega)}$	$2k_o^{(\omega)}+\bar{k}_o^{(\omega)}=k_o^{(3\omega)}-2Q$	$2\kappa_+^{(\omega)}+\bar{\kappa}_-^{(\omega)}=\kappa_-^{(3\omega)}$	1.4
12.	$3k_+^{(\omega)}=k_+^{(3\omega)}$	$3k_o^{(\omega)}=k_o^{(3\omega)}-Q$	$3\kappa_+^{(\omega)}=\kappa_+^{(3\omega)}-Q$	17
13.	$3k_+^{(\omega)}=k_-^{(3\omega)}$		$3\kappa_+^{(\omega)}=\kappa_-^{(3\omega)}+NQ$	* $\varepsilon_\eta^{1/2}(3\omega) \geq \varepsilon_\xi^{1/2}(\omega)$
14.	$2k_+^{(\omega)}+k_-^{(\omega)}=k_-^{(3\omega)}$		$2\kappa_+^{(\omega)}+\kappa_-^{(\omega)}=\kappa_-^{(3\omega)}+NQ$	* $3\varepsilon_\eta^{1/2}(3\omega) \geq 2\varepsilon_\xi^{1/2}(\omega)+\varepsilon_\eta^{1/2}(\omega)$
15.	$k_+^{(\omega)}+2k_-^{(\omega)}=k_-^{(3\omega)}$		$\kappa_+^{(\omega)}+2\kappa_-^{(\omega)}=\kappa_-^{(3\omega)}+NQ$	* $3\varepsilon_\eta^{1/2}(3\omega) \leq \varepsilon_\eta^{1/2}(\omega)+2\varepsilon_\eta^{1/2}(\omega)$

* Condition for Phase

	Mode Combination for Phase Matching	Concentration of Cholesteryl Chloride	$\bar{\varepsilon}(\omega)$	$\bar{\varepsilon}(3\omega)$	α	Predicted Pitch for Phase Matching
1.	$k_+^{(\omega)}+2k_-^{(\omega)}=\bar{k}_-^{(3\omega)}$	0 (%)	2.17±0.01	2.27±0.01	0.027±0.002	-237±2 nm
2.	$3k_-^{(\omega)}=\bar{k}_+^{(3\omega)}$					
3.	$\bar{k}_+^{(\omega)}+2k_-^{(\omega)}=\bar{k}_+^{(3\omega)}$					
4.	$k_+^{(\omega)}+\bar{k}_+^{(\omega)}+k_-^{(\omega)}=\bar{k}_-^{(3\omega)}$	22	2.18	2.29	0.028	-352±2 nm
5.	$2k_-^{(\omega)}+\bar{k}_-^{(\omega)}=\bar{k}_-^{(3\omega)}$					
6.	$3k_-^{(\omega)}=\bar{k}_-^{(3\omega)}$	30	2.18	2.30	0.027	-472±3 nm
7.	$2k_+^{(\omega)}+\bar{k}_-^{(\omega)}=k_+^{(3\omega)}$					
8.	$k_+^{(\omega)}+k_-^{(\omega)}+\bar{k}_-^{(\omega)}=k_-^{(3\omega)}$	40	2.19	2.31	0.030	-689±5 nm
9.	$2k_+^{(\omega)}+\bar{k}_+^{(\omega)}=k_-^{(3\omega)}$					
10.	$\bar{k}_+^{(\omega)}+2k_-^{(\omega)}=\bar{k}_-^{(3\omega)}$					
11.	$2k_+^{(\omega)}+\bar{k}_-^{(\omega)}=k_-^{(3\omega)}$	48	2.20	2.32	0.030	-1377±10 nm
12.	$3k_+^{(\omega)}=k_+^{(3\omega)}$	‡	2.19	2.30	0.029 0.027	-17.3±1 μm +17.4±1 μm

‡ Mixture of 1.75 parts of cholesteryl chloride and 1 part of cholesteryl myristate by weight.

Table II

Mode Combination for Phase Matching	Predicted Phase-Matching Temperature	$\frac{dp}{dT}$	Observed Phase-Matching Temperature	Relative Phase-Matched Third-Harmonic Intensity
1. $k_+^{(\omega)}+2k_-^{(\omega)}=\bar{k}_-^{(3\omega)}$	38±3 (°C)	0.7 (nm/°C)		
2. $3k_-^{(\omega)}=\bar{k}_+^{(3\omega)}$			39.5 (°C)	2×10^{-4}
3. $\bar{k}_+^{(\omega)}+2k_-^{(\omega)}=\bar{k}_+^{(3\omega)}$			30.5	1×10^{-2}
4. $k_+^{(\omega)}+\bar{k}_+^{(\omega)}+k_-^{(\omega)}=\bar{k}_-^{(3\omega)}$	32±2	1.3		
5. $2k_-^{(\omega)}+\bar{k}_-^{(\omega)}=\bar{k}_-^{(3\omega)}$			30.5	3×10^{-3}
6. $3k_-^{(\omega)}=\bar{k}_-^{(3\omega)}$	38.2±1	3.6	38.1	1×10^{-4}
7. $2k_+^{(\omega)}+\bar{k}_-^{(\omega)}=k_+^{(3\omega)}$			29.9	3×10^{-1}
8. $k_+^{(\omega)}+k_-^{(\omega)}+\bar{k}_-^{(\omega)}=k_-^{(3\omega)}$	30.1±0.6	8.5		
9. $2k_+^{(\omega)}+\bar{k}_+^{(\omega)}=k_-^{(3\omega)}$			29.9	1×10^{-2}
10. $\bar{k}_+^{(\omega)}+2k_-^{(\omega)}=\bar{k}_-^{(3\omega)}$	31.1±0.6	8.5	31.2	3×10^{-2}
11. $2k_+^{(\omega)}+\bar{k}_-^{(\omega)}=k_-^{(3\omega)}$	33.3±0.3	39	33.6	4×10^{-4}
12. $3k_+^{(\omega)}=k_+^{(3\omega)}$	49.4±0.2 54.2±0.2	6400	49.3 54.1	1 1

Table III

Mode Combination for Phase Matching	$\frac{d(\Delta k)}{dp}$	$\frac{\delta p_1}{p}$	$\frac{\delta p_2}{p}$	$\frac{\delta p_3}{p}$	$\frac{\delta p_4}{p}$	Predicted Width	Observed Width
2. $3\bar{k}^{(\omega)}=\bar{k}^{(3\omega)}$	$220(\mu m^{-2})$	4.0×10^{-4}	9.1×10^{-4}	7.5×10^{-3}	8×10^{-5}	3.0 (°C)	2.8 (°C)
3. $\bar{k}^{(\omega)}+2\bar{k}^{(\omega)}=\bar{k}^{(3\omega)}$	100	9.5×10^{-4}	1.4×10^{-3}	7.5×10^{-3}	7×10^{-5}	2.2	1.7
6. $3\bar{k}^{(\omega)}=\bar{k}^{(3\omega)}$	110	4.6×10^{-4}	1.8×10^{-3}	7.5×10^{-3}	8×10^{-5}	1.3	1.0
7. $2\bar{k}^{(\omega)}+\bar{k}^{(\omega)}=\bar{k}^{(3\omega)}$	27	1.3×10^{-3}	2.6×10^{-3}	7.5×10^{-3}	7×10^{-5}	0.7	0.6
11. $2\bar{k}^{(\omega)}+\bar{k}^{(\omega)}=\bar{k}^{(3\omega)}$	13	5.8×10^{-4}	5.3×10^{-3}	7.5×10^{-3}	7×10^{-5}	0.4	0.4
12. $3\bar{k}^{(\omega)}=\bar{k}^{(3\omega)}$	0.04	3.3×10^{-2}	6.7×10^{-2}	7.5×10^{-3}	5×10^{-3}	0.3	0.3

Table IV

TECHNICAL INFORMATION DIVISION
LAWRENCE BERKELEY LABORATORY
UNIVERSITY OF CALIFORNIA
BERKELEY, CALIFORNIA 94720